Estimating Impact of Age Distribution on Bond Pricing: A Semiparametric Functional Data Analysis Approach*†

Zongwu Cai[a], Jiazi Chen[b] and Linlin Niu[b,c,†]

[a]Department of Economics, University of Kansas, Lawrence, KS 66045, USA

[b]The Wang Yanan Institute for Studies in Economics, Xiamen University, Xiamen, Fujian 361005, China

[c]MOE Key Lab of Econometrics and School of Economics, Xiamen University, Xiamen, Fujian 361005, China

September 13, 2021

Abstract: This paper proposes a semiparametric functional data model to estimate the impact of demographic age distribution on interest rate term structure through an innovative functional affine term structure, which fully exploits the information efficiency in both structures. The framework consistently explains the age distribution impact on the persistence in yields via both channels of real rate and inflation, supporting the long run Fisher relationship and the life cycle hypothesis. Structural information in yields also helps to strongly identify the demographic impact function, which results in remarkable fit of the yield curve with counter-cyclical risk premia and more accurate out-of-sample forecast than alternative models.

Keywords: Demographic distribution; Dynamic yield curve; Functional data analysis; Life cycle; Term structure models; Semiparametric modeling.

1 Introduction

High persistence (trend) is a well-known stylized fact in charactering interest rates dynamics and imposes theoretical and empirical challenges in yield curve modeling. Techni-

*We thank Professors Thomas Sargent, Harald Uhlig, and Haoxi Yang for their valuable comments and discussions, and all seminar and workshop participants at Xiamen University, Zhejiang University, National Chung Hsing University, Monash University, Hunan University, Southwestern University of Finance and Economics, the Shanghai Academy of Social Sciences, Northeastern University of Finance and Economics, and Peking University. This research was partially supported by the National Natural Science Foundation of China with grant numbers 71631004, 71871193, and 72033008.

†Corresponding author: Linlin Niu. Email: llniu@xmu.edu.cn.

cally, modeling the trend characteristic in the interest rate term structure is essential for predicting yields and understanding risk premia. Theoretically, understanding the fundamental mechanism behind the trend is of great importance for macroeconomic research, investment strategies and economic policy making.

Changing demographic factor has been proposed as a candidate to explain the trend in yields with economic underpinnings and some empirical validity, but its explanatory power may be sensitive to the age cohort composition in constructing demographic factor and its empirical performance varies with samples. Moreover, in terms of influencing channels of demographic impact on yields, the existing literature made more extensive studies on the channel of real rate than on inflation, though both of which are underlying the dynamics of the nominal yields. A thorough examination on the demographic influence on both channels with structural consistence is still lacking.

This paper proposes a unified framework to address the above issues with a functional perspective to link the demographic age structure with interest rate term structure. The functional approach provides a full-range view on the life-cycle impact of demographic age structure on real rate, inflation, and short-term nominal rate in line with a long run Fisher relationship and the life cycle hypothesis. Meanwhile, utilizing the cross-maturity information in the term structure improves the efficiency to infer a highly significant demographic impact function on nominal yields with robustness. The resulting functional affine arbitrage-free term structure model (FATSM) decomposes yields into a slow-moving trend driven by demographic age structure and a business cycle autoregressive component. Applying the model to U.S. Treasury yield curve with age distribution produces remarkable in-sample fit with countercyclical risk premia and accurate out-of-sample prediction. It implies a persistently low level of yield trend driven by the demographic age structure in the forthcoming decade.

1.1 Term Structure of Interest Rates: Trend Beyond the Business Cycle

The trending behavior of yields beyond the business cycle fluctuation can be visualized from a life-long span of interest rate term structure as shown in Figure 1, which presents a three-dimensional plot of the U.S. Treasury yield curve from 1952:Q2 to 2018:Q1. The data are the 3-month Treasury T-bill rates from the Federal Reserve, and 1-year to 5-year Fama-Bliss zero-coupon equivalent Treasury yields from the CRSP database. These data provide a relatively long span of sample compared to other choices. During this period of nearly seven decades, fluctuations in the business cycle, which usually last between

a few years and about a decade, seem doomed by the large swing starting from a low percentage in the 1950s, rising to a double-digit high in the 1970s and 1980s, then sliding down for more than three decades until the recent era of "zero lower bound" (ZLB). In addition, this persistence in the interval of a few decades is difficult to be justified by a mean-reverting process with a constant long-term mean. To characterize a non-constant long-term mean, for example, Balduzzi et al. (1998) explore the idea of a stochastic central tendency of short-term interest rate and its expected information in long term yield to better forecast short rate, whereas based on the relationship between yields and forward spreads over a long period starting from 1952, Fama (2006) also provides strong evidence to suggest a non-stationary long-term mean and local mean-reverting process throughout the business cycle.

[Figure 1: U.S. Treasury yield curve from 1952:Q2 to 2018:Q1]

In the vast literature on interest rates and yield curve modeling, however, most studies have relied on the assumption of a constant long-term mean, since the pioneering work on no-arbitrage dynamic term structure models initiated by Vasicek (1977) and Cox et al. (1985), in particular, the reduced form popularized by Diebold and Li (2006) or the macro-finance models developed by Ang and Piazzesi (2003). By recognizing the persistent feature of yields and the related small-sample bias of parameter estimation under constant long-term mean, Bauer et al. (2012) propose a method for bias-corrected estimates. However, bias correction under constant mean is insufficient to avoid misspecification problems under time-varying long-term mean, and the resulting forecast tends to under-predict when the yields in the chosen sample are trending upward, or to over-predict with a downward trend. As long-term yields are the risk-adjusted average of future short-term rates, under-predicting (over-predicting) future short-term rates results in overpricing (underpricing) risk premia. In macro-finance research, misspecification of the long-term mean of short-rates may lead to estimation bias for the economic mechanism behind the determination of interest rates.

These drawbacks of trend misspecification have called for research on the introduction of time-varying means in state dynamics of yield modeling. One approach is to use long-memory processes to describe state dynamics, such as cointegrated vector autoregression in reduced form as in Bowsher and Meeks (2008) or with no-arbitrage restrictions as proposed by Goliński and Zaffaroni (2016) and Bauer and Rudebusch (2020), which outperform random walk models for short horizons or alternative short-memory models. An alternative approach is to introduce regime switching as in Ang and Bekaert (2002) and Bansal and Zhou (2002), although it is not flexible enough to accommodate a sequence

of permanent shocks as shown in Fama (2006). Using adaptive autoregressive models is another approach to reflect the global time-varying mean with a local stationary process with flexibility, parsimony, and desirable forecasting property as studied by Zantedeschi et al. (2011) and Chen and Niu (2014). Introducing external persistent measures beyond yield information also provides a way to proxy the trend behavior of yields as in Cieslak and Povala (2015).

In the literature on the macro-finance term structure, efforts have been made to investigate the fundamental sources of stochastic trends in yields. According to the Fisher equation, trends in inflation and real interest rates are natural candidates underlying the trends in nominal interest rates. For example, Cieslak and Povala (2015) take the discounted moving average of past inflation to proxy the adaptive expectation of inflation as the major source of yield trends and find that the resulting cyclical component of yields can predict changes in short-rates and excess bond returns. Also, Duffee (2018) points out the relative importance of shocks to real rates and term premia in explaining yield variances. Finally, Bauer and Rudebusch (2020) find that the two "falling stars," the falling inflation trend during the 1980s and 1990s and the falling real rate trend over the last two decades, can explain the persistent decline in nominal yields over the last 40 years. Yet the drivers of these falling stars remain to be investigated further.

1.2 Demographic Age Structure: Mechanism and Measurement

1.2.1 Impact Channels of Demographic Age Structure on Nominal Yields

Theoretically, the trend of nominal yields is composed of trends in real interest rate and inflation according to a long run Fisher relationship. The relationships between a population's demographic age structure, real rates and inflation have been studied in the literature both analytically and empirically.

Thorough study on the demographic mechanism affecting real rate goes back to Modigliani (1966), which provides an analytical foundation for the life cycle impact of the age structure of the population on real rates through aggregate savings. The life cycle theory predicts that when population growth exceeds the stationary level for successive years, the high proportion of baby boomers in the population will lead to a higher ratio of working-age households in their wealth accumulation phase, thus causing excessive aggregate saving; later in their de-saving phase, the same cohorts will lead to a higher ratio of older households, thus reducing aggregate saving. Excess savings tend to lower interest rates and asset returns, and a savings shortage tends to increase returns. Moreover, an aging population and longevity risk tend to further increase savings or to prolong

the saving phase before retirement and decrease labor supply with falling productivity growth(Bloom et al., 2003; Zhang et al., 2003; Cocco and Gomes, 2012; Carvalho et al., 2016; Cooley and Henriksen, 2018; Gagnon et al., 2021). Both population growth and the higher life expectancy of baby boomers can translate into lower real rates during their working age. Various studies have demonstrated that the U.S. baby boom from the end of World War II to the 1960s and the increase in life expectancy had a significant impact on the macro economy and real returns[1] .International studies confirm a similar pattern (Ang and Maddaloni, 2005; Aksoy et al., 2019; Papetti, 2021) globally.

In terms of demographic influence on inflation, although less studied than the demographic link to real rates via savings, there is an empirical evidence on the correlation between changing demographic structure and inflation in the U.S. (McMillan and Baesel, 1990) and in OECD countries (Lindh and Malmberg, 2000; Juselius and Takáts, 2021). Possible mechanisms of fiscal redistribution across generations have been proposed to explain this phenomenon (Bullard et al., 2012; Katagiri et al., 2020). Moreover, Goodhart and Pradhan (2020) builds a between the global demographic structural change, including the drastic demographic change in China, and trends of inflation and inequality. Therefore, to the best of our knowledge, there has not been a consistent explanation on demographic age impact on interest rates through real rate and inflation at the same time.

1.2.2 Measurement on Demographic Age Structure

In analytical studies on demographic impact on interest rate, inflation, or asset returns, tractability calls for simple measures of demographic structure. Thus, population is often divided roughly into two or three generations such as young, middle aged and retirees, out of which simple measures of the demographic structure can be characterized by the proportion of a generation or a ratio between them. For example, Geanakoplos et al. (2004) propose a single index, termed as the MY ratio between the middle-aged population (40-49) and the young population (20-29) as a proxy for the demographic structure to study its impact on the long-run pattern of U.S. asset returns based on an overlapping generation (OLG) model. The MY ratio has been conveniently used in a sequence of studies on the demographic impact on stock returns, inflation, and interest rates (Favero et al., 2011, 2016; Gozluklu and Morin, 2019). In particular, Favero et al. (2016) derive a no-arbitrage term structure model based on the argument that the short-rate follows a Taylor rule based on the time-varying demographic factor of MY and present supporting

[1]See, for example, Bakshi and Chen (1994), Abel (2003), Goyal (2004), Krueger and Ludwig (2007), DellaVigna and Pollet (2007), Favero et al. (2011),Lunsford and West (2019), and among others.

evidence of its significant impact on the whole yield curve.

However, the single index approach to characterize the demographic age structure has empirical drawbacks. In the simple index, a generation usually consists of a range of age cohorts defined by rule-of-thumb. The corresponding empirical results are not robust to different age cohort compositions in a generation (Poterba, 2001) and fails to explain the persistently low interest rate over the last two decades (Del Negro et al., 2019). It is also inefficient to characterize the entire age distribution by excluding the very young and the very old population. Like many life cycle analyses, data on younger age cohorts before entering the labor force are missing from the MY ratio. As the younger cohorts consume the accumulated savings of the dependent family, they may have an important impact on a household's economic and portfolio decisions (Browning and Ejrnæs, 2009; Love, 2010; Hubener et al., 2016). Thus, an unusually high or low proportion of younger cohorts will affect aggregate savings and asset returns, which can not be captured by the MY ratio.

To further examine the impact of the age distribution of the population on the macro economy, Fair and Dominguez (1991) propose a linear parametric model allowing non-linear effect with second order degree polynomial to estimate the age effects of 55 age-groups in U.S. macroeconomic equations of consumption, investment, money-demand, and employment. Using similar approach with international panel data, Higgins (1998) examines the relationship between age distribution, national savings and the current account balance, and Juselius and Takáts (2021) study the demographic effect on inflation and monetary policy. But the inference of the parametric method suffers from potential nonstationarity problem of the time series and possible misspecification of functional form. Moreover, the employed polynomial form of age coefficients may not be fully flexible to capture the intrinsically complex relationship between variables, and the choice of polynomial form is arbitrary without a formal selection criteria.

To overcome the aforementioned problems for a parametric model, Park et al. (2010) proposes a semiparametric cointegration regression model with an efficient estimator which contains a nonparametric component of age distribution with a functional form of impact coefficient based on Fourier flexible form (FFF) approximation. This model is parsimonious with a few parameters in the FFF approximation to capture the nonlinear impact of age along the life cycle, and the number of parameters can be properly chosen with a specification test. Applying the model to U.S. data, Park et al. (2010) finds the age distribution impact on consumption and savings rate takes a U-shape and an inverted U-shape respectively, which is in line with the life-cycle hypothesis and performs better than the parametric method.

1.2.3 A Functional Perspective on the Dynamic Linkage Between the Two Structures

Based on the review on interest rate trend modeling and analysis using demographic age structure as explanatory variable, we find that it is promising to employ the functional perspective of the age distribution as a building block for yield curve modeling.

By doing, we first make single equation analysis on the age distribution impact on real interest rate, inflation, and nominal short rate, respectively. If the Fisher equation holds in the long run in terms of the life-cycle horizon, the shape of the impact function on nominal short rate should be consistent with the sum of age impacts in real rate and inflation, thus explaining the demographic age structure impact on nominal yield through both channels of real rate and inflation. Testing the stationarity of the residuals in the single equation regression demonstrates whether the cointegration relationships between age distribution and the related series can explain the long run trend and filter out business cycle fluctuations.

Based on the short rate regression results, we then build a joint model of the interest rate term structure with a trend driven by age distribution and local mean-reverting processes in a unified functional affine arbitrage-free term structure model. We show that the term structure information substantially improves the efficiency in the estimation of the age impact function of nominal short rate, which in turn helps to fit and forecast the yield curve remarkably well.

This paper contributes to the macro-finance literature in the following four ways. First, the proposed model consistently explains the slow-moving trend of the yield curve through a life cycle component that drives both real rate and inflation trends. It implies a more intuitive spanning mechanism driving the "falling stars" for short- and long-term horizons through expectations, compared to the latent unspanned mechanism proposed in Bauer and Rudebusch (2020). The rich information provided by the yield curve offers more robust inferences about the natural interest rate for policy recommendations than results derived from dynamic stochastic general equilibrium models relying on limited macroeconomic sample information (Eggertsson et al., 2019).

Second, the functional approach is more efficient and robust to utilizing the entire age distribution to explain the trend in yields than the single index approach summarizing the demographic structure with simple indicators such as the MY ratio (Favero et al., 2016). Our model performs better both in- and out-of-sample when it is compared to a counterpart affine arbitrage-free model with the MY ratio as explanatory variable. Although we do not explicitly model the time-varying trend as a Taylor rule element to construct the no-arbitrage term structure model, it is generally compatible and flexible to incorporate

alternative macro-finance specifications, such as adapting to a Taylor rule setting for the short rate targeting on a time-varying trend driven by demographic age distribution.

Third, methodologically, we show the mutual efficiency brought about by the cross-equation restrictions in the term structure to improve the estimation accuracy of the life cycle age impact function. In previous research, the impact function of the demographic age distribution is generally estimated for various macroeconomic variables using a single equation; see, for example, Fair and Dominguez (1991), Higgins (1998), Park et al. (2010), and Park (2010) for details. However, due to limited data on typical macroeconomic time series, parameter inference and the choice of specifications are subject to uncertainty in a small sample. In the application of our functional affine term structure model, the resulting life cycle age impact function are more reliable with higher statistical significance, which then contributes to higher accuracy in out-of-sample yields prediction compared with performance of alternative popular models.

Finally, technically, the model is set up in a semiparametric representation under the functional affine arbitrage-free assumption. Compared with previous semiparametric dynamic term structure models without macroeconomic foundation or theoretical restrictions, such as the models in Ghysels and Ng (1998) and Härdle and Majer (2016), our proposed model demonstrates the possibility of introducing the nonparametric method for structural macro-finance analysis. We show that the functional impact of the demographic age distribution can be approximated nonparametrically by using the Fourier flexible expansion (FFE) proposed by Park et al. (2010) not only in the single short rate equation, but also in structural equations of the yield curve under the no-arbitrage assumption. In this affine arbitrage-free framework, the nonlinearity of the factor loadings in the measurement equations usually makes the estimation difficult both in terms of determining the global optimum and parameter uncertainty. To overcome this difficulty, the Bayesian approach of the Markov chain Monte Carlo (MCMC) method is used to estimate the related parameters in the proposed model.

In summary, our novel functional affine approach addresses the theoretical and empirical challenges of modeling the interest rate term structure with persistent trends driven by the fundamental of demographic age structure.

The rest of this paper is organized as follows. Section 2 presents empirical evidence of the impact of the age distribution on real rates, inflation, and short term nominal yield consistent with the life-cycle hypothesis and a long-run Fisher relationship. Section 3 develops the functional affine arbitrage-free interest rate term structure model with a time-varying mean driven by the age distribution of the population. Section 4 describes the estimation strategy using the Bayesian method. Section 5 discusses the empirical results

of the model and demonstrates its excellent properties of yield fitting, decomposition and forecasting performance. Section 6 concludes the study.

2 Age Impact Analysis on Nominal Short Rate

After intuitively visualizing the most visible generations outweighing others in the U.S. slow-moving age distribution, this section presents the single equation functional regression to learn the life-cycle impact of age distribution by separately regressing the real rate r_t, inflation π_t, and the nominal short-term yield i_t on the age distribution of the population. The results support a long-run Fisher relationship between the trends.

2.1 A Bird's Eye View on the Age Distribution: Waves of Generations

To visualize the bulky weight and possible impact of baby boomers in the population and their slow movement over time, the age distribution of the U.S. population based on annual data is plotted in Figure 2, which can be downloaded from the U.S. Census Bureau and it covers each age bin (from under 1 to 85 and over) from 1940 to 2018. At each time point, the weight of each age cohort is computed relative to the total population. As shown in Figure 2, the weight of the baby boomer cohort is the most obvious feature in both dimensions: over time, and baby boomers stand out as an increase in infant weight at the lower end of the age distribution after World War II for about 20 years. Then, as they move through different life stages, these cohorts form a persistent wave-like pattern across the age distribution. An implication of this pattern is that the economic behavior of baby boomers is more important at the aggregate level. In turn, their change in behavior over the life cycle can slowly alter macroeconomic variables, including asset returns.

[Figure 2: Dynamics of the age distribution of the U.S. population]

Besides the baby boomers, small waves of other generations also exist, such as those local peaks from echo boomers born during 1985-2004, mirroring the birth rate peaks of the baby boomer generation 20 years later.

According to the life-cycle theory, individual generations exhibit life-cycle patterns of economic decisions and activities such as an inverted U-shape savings along life. Should the population consist of balanced generations with equal birth rate and survival rate, the aggregate savings and other variables associated with life-cycle decisions become constant because of social balance across generations. If some generations outweigh others due

to higher birth rate, their decision pattern would affect the aggregate level accordingly. Once we have a long span data of age distribution, the functional regression can help us to learn the life-cycle impact of age distribution on various economic variables.

2.2 Trend Decomposition with a Demographic Factor of a Functional Form

We are interested in the life-cycle impact of age distribution on short term interest rate and on their components of real rate and inflation, respectively. It is assumed that each economic variable, denoted by x_t for the general elaboration, is composed of a time-varying long-term trend x_t^* and an autoregressive component $\tilde{x}_t$, which reflects fluctuations at the business cycles and higher frequencies and reverts to the long-term mean x_t^* as follows:

$$x_t = x_t^* + \tilde{x}_t,$$

and x_t^* is driven by an aggregate life cycle component resulting from the age distribution of the population multiplied by its impact $g(s)^x$ as follows

$$x_t^* = \int_{\underline{S}}^{\bar{S}} f_t(s) g^x(s) ds, \tag{2.1}$$

which is a functional data analysis model (see, for example, Ramsay and Silverman (1997) and Park et al. (2010) for details), where the age range is $s \in [\underline{S}, \bar{S}]$, $f_t(s)$ denotes the density function of the demographic distribution at time t, and $g^x(s)$ represents the age impact function related to x_t. This function has two implications: each cohort has an impact $g^x(s)$ at age s and the shape of $g^x(s)$ over the life span $s \in [\underline{S}, \bar{S}]$ reflects a life cycle pattern; at each period t, the aggregate impact of the population on x_t is the integral of the age density multiplied by the age impact $g^x(s)$ across all age cohorts over the life span.

Then, based on the Fisher equation giving the short nominal rate as the sum of the real rate and inflation,

$$i_t = r_t + \pi_t,$$

it is reasonable to assume that the Fisher equation relationship should hold for both the time-varying long-term mean and the cyclical terms:

$$i_t^* = r_t^* + \pi_t^* \quad \text{and} \quad \tilde{i}_t = \tilde{r}_t + \tilde{\pi}_t.$$

Next, based on a common age factor $f_t(s)$ and the functional form of (2.1), the implication of the impact function is decomposed as

$$g^i(s) = g^r(s) + g^\pi(s).$$

Therefore, the age impact functions of real rates and inflation add up to the impact function of nominal yields.

To estimate the impact function $g(s)$, there are many methods available in the literature, such as the series method as

$$g(s) = \sum_{i=1}^{\infty} \alpha_i \psi_i(s),$$

where $\{\psi_i(s)\}$ is a sequence of (orthogonal) basis functions. For simplicity, motivated by the idea developed in Park et al. (2010), we use a semiparametric method to approximate $g(s)$ with a Fourier flexible series as follows:

$$g_\kappa(s) = \sum_{i=1}^{\kappa} \alpha_i \psi_i(s) = \alpha_1 + \alpha_2 s + \alpha_3 s^2 + \sum_{j=1}^{J} \left[\alpha_{4,j} \cos(js) + \alpha_{5,j} \sin(js)\right], \tag{2.2}$$

where $\kappa = 3 + 2J \to \infty$, indicating the number of parameters in the approximating function $g_\kappa(s)$, by assuming that $\|g_\kappa(s) - g(s)\| \to 0$ as $\kappa \to \infty$.

Remark 1. *As the age impact function contains the trigonometric series, it is desirable to scale the age range to the interval* $[0, 1]$. *That is, with a given common support* $s \in [\underline{S}, \bar{S}]$ *for* $f_t(s)$, $f_t(s)$ *becomes* $f_t^*(s^*) = f_t[\underline{S} + (\bar{S} - \underline{S})s^*]$, *with the common support* $s^* \in [0, 1]$. *The original impact function* g *with respect to* f_t *can be retrieved from the impact function* g^* *with respect to* f_t^* *by the following transformation* $g(s) = g^*[(s - \underline{S})/(\bar{S} - \underline{S})]$. *Finally, note that one might use a B-spline to approximate* $g(s)$ *or a nonparametric (kernel estimation) procedure or a Baysian spline; see Ramsay and Silverman (1997) and Kowala et al. (2017) for details.*

The reason for choosing the FFE method is that, as illustrated in Park et al. (2010), this FFE approximation may be more parsimonious than other parametric methods, which often suffer from the typical multicollinearity problem, and it has an intuitive interpretation for the selected Fourier series at different frequencies. It is also more efficient with an asymptotic distribution, as shown in Andrews (1991), than other methods such as the parametric polynomial approximation in Fair and Dominguez (1991). Thus, plugging

(2.2) into (2.1) leads to the following result:

$$x_t^* = \int_0^{\bar{S}} f_t(s)g(s)ds \approx \sum_{i=1}^{\kappa} \alpha_i \int_0^{\bar{S}} f_t(s)\psi_i(s)ds. \tag{2.3}$$

Next, by dividing the age support $[0, \bar{S}]$ into M age sub-intervals, $[0, s_1), \ldots, [s_{m-1}, s_m)$, $\ldots, [s_{M-1}, \bar{S}]$, each with a weight

$$w_t(s_m) = \int_{s_{m-1}}^{s_m} f_t(s)ds,$$

the integral in (2.3) can be simply approximated as

$$\int_0^{\bar{S}} f_t(s)\psi_i(s)ds \approx \sum_{m=1}^{M} w_t(s_m)\psi_i(\bar{s}_m) \tag{2.4}$$

with $\bar{s}_m = (s_{m-1} + s_m)/2$.

2.3 Linear Estimator

Based on the approximation in (2.4), (2.3) can be written in the following simple linear form

$$x_t^* = \alpha' z_t, \tag{2.5}$$

where $\alpha = (\alpha_1, \cdots, \alpha_\kappa)'$ and $z_t = (z_{t1}, \cdots, z_{t\kappa})'$ with $z_{ti} = \sum_{m=1}^{M} w_t(s_m)\psi_i(\bar{s}_m)$ for $1 \leq i \leq \kappa$. Given x_t and z_t, α can be estimated with an ordinary least squares (OLS) estimator $\widehat{\alpha}$, from which the age impact function can be inferred as

$$\widehat{g}_\kappa(\bar{s}_m) = \widehat{\alpha}' \, \Psi(\bar{s}_m), \tag{2.6}$$

where $\Psi(\bar{s}_m) = (\psi_1(\bar{s}_m), \cdots, \psi_\kappa(\bar{s}_m))'$ at $\bar{s}_m$ for $1 \leq m \leq M$. The $\kappa \times \kappa$ variance-covariance matrix of $\widehat{\alpha}$, $\text{var}(\widehat{\alpha})$, can be obtained from the regression residuals through the heteroscedasticity and autoregressive consistent (HAC) procedure in Newey and West (1987), and the $M \times M$ variance-covariance matrix of the age impact function, $\text{var}(\widehat{g_\kappa})$, can be computed easily as follows:

$$\text{var}(\widehat{g}_\kappa) = \Psi_\kappa' \text{var}(\widehat{\alpha}) \Psi_\kappa, \tag{2.7}$$

where $\widehat{g}_\kappa = (\widehat{g}_\kappa(\bar{s}_1), \cdots, \widehat{g}_\kappa(\bar{s}_M))' = \Psi_\kappa' \widehat{\alpha}$ and $\Psi_\kappa = (\Psi(\bar{s}_1), \cdots, \Psi(\bar{s}_M))$ is a $\kappa \times M$ matrix.

To choose the optimal κ, following Park (2010), it is assumed that the dependent

variable and the regressors have no stochastic trends and, use the h-block cross-validation (HCV) and the modified h-block CV (MHCV) criteria as proposed by Burman et al. (1994) and Racine (1997). For any given block size h, the HCV criterion is given by

$$\text{HCV} = \frac{1}{T}\sum_{t=h}^{T-h}\left[x_t - z_t'\widehat{\alpha}(t,h)\right]^2,$$

where T is the number of original observations. The estimator $\widehat{\alpha}(t,h)$ is obtained by removing the t-th observation and the h observations before and after the t-th observation in the two sequences of $\{x_t\}$ and $\{z_t\}$. As suggested by the simulation study of Burman et al. (1994), h can be simply set to $h = T/6$. However, when the ratio κ/T is not trivial, it is better to use the MHCV criterion, which can have the following form:

$$\text{MHCV} = \text{HCV} + \frac{1}{T^2}\sum_{t=h}^{T-h}\sum_{s=1}^{T}\left[x_s - z_s'\widehat{\alpha}(t,h)\right]^2 + \frac{1}{T}\sum_{t=1}^{T}(x_t - z_t'\widehat{\alpha})^2.$$

Thus, the best κ can be chosen by minimizing the two CV criteria above.

2.4 Empirical Results of Single Equation Regressions

We use U.S. data to estimate the age impact functions for consumer price index (CPI) inflation, the 3-month Treasury yield, and the ex post real rate, calculated using the 3-month nominal yield minus actual realized inflation. The annual age distribution of population based on the U.S. Census Bureau is represented in Figure 2. To match the quarterly frequency of the three macroeconomic series, we interpolate the annual distribution to obtain the quarterly distribution based on the assumption that the quarterly birth rates and quarterly death rates have no seasonality in a year, so that we can compute these quarterly rates from their corresponding annual rates. As a preliminary study, for each economic variable, we run a regression on the age distribution to obtain a related age impact function. With the MHCV criterion, κ is set to 5 for both inflation and the nominal rate. Although the selected κ is set to 2 for the real rate in a single equation study, we set it to 5 to incorporate the economic restrictions of the Fisher equation without imposing cross-equation restrictions on parameter values in the regression. Figure 3 presents the resulting age impact functions.

[Figure 3: Age impact functions of single equation regressions]

In Figure 3, the left panel depicts the age impact functions for inflation as a dashed line, for the real rate as a dotted line. The age impact function for the real rate exhibits a

U-shaped curve, mirroring the inverted U-shaped curve of the impact function for savings found in Park et al. (2010), consistent with the life cycle hypothesis. The age impact function for inflation has an inverted U-shaped curve, with different impacts for the young, middle-aged, and older population. The negative impact of the older population on inflation is consistent with the deflationary effect in a politico-economic equilibrium (Bullard et al., 2012; Katagiri et al., 2020). Empirically, a U-shaped impact for consumption has been found by Park et al. (2010), and a money demand equation with constant money supply growth can lead to such an inverted-U shape age impact on inflation if output growth coincides with consumption growth in equilibrium and the latter trend is driven by the demographic age distribution.

Although the U-shaped function for the real rate and the inverted U-shaped function for inflation face to opposite directions, they are not symmetrical with respect to the zero line and their sum represents a S-shaped function for the nominal short rate, indicated by circles on the right panel of Figure 3. The right panel also plots the age impact function estimated directly for the nominal short rate in solid line which almost coincides with the implied function marked with circles. The 95% confidence interval shows that the impact function is significantly positive for the young population (aged 10 to 35) and significantly negative for the middle-aged and older population (aged 45 to 73).

According to (2.1), the time-varying trend can be computed as the integral of the age distribution multiplied by the impact function. With the results of the impact functions above, this integral amounts to computing the sum of the products of the discretized age density and its impact for each age group. Figure 4 plots the resulting trends for each variable. The left panel plots the trends for inflation as a dashed line and for the real rate as a dotted line, and their sum is depicted with circles in the right panel to indicate the implied trend for the nominal rate. The right panel also plots the trend of the nominal short rate computed directly from the regression results in solid line and contrasts it with the actual nominal rate. Nonstationarity are rejected by ADF test for all three residual processes after removing the trends driven by age distribution, which validates the cointegration relationship between the demographic age distribution and the original series.

[Figure 4: Demographic trends of single equation regressions]

The following three observations emerge from the above analysis:

1. The demographic trend of inflation is downward from the mid- 1970s and stabilizes around the mid-1990s. The trend in the real rate declines continuously from the

mid-1990s. These "falling stars" patterns are similar to those findings in Bauer and Rudebusch (2020), which do not explain the mechanism behind.

2. It is strongly evident that the demographic trend of the nominal rate follows the actual rate closely and smoothly.

3. The directly computed trend in the right panel is consistent with the indirectly computed trend based on its components from the left panel, supporting the Fisher equation under low frequency.

We also regress these series on the simple demographic factor of MY ratio (Geanakoplos et al., 2004; Favero et al., 2016; Lunsford and West, 2019; Del Negro et al., 2019; Gozluklu and Morin, 2019), and the resulting impact coefficients on inflation, real rate and nominal short rate are -9.635, -2.028 and -11.662, respectively. The sum of the first two closely matches the latter. The fitted trends of the three series are shown in Figure 5, where discrepancies arise mainly for the last two decades that the MY ratio can not explain the falling trend of real rate and flat trend in inflation. The resulting prediction for the nominal rate is an upward trend after 2000, departing from the actual path persistently.

[Figure 5: Trends explained by the MY ratio]

The above single equation analysis demonstrates that the functional approach provides robust measures on the demographic age structure. The results from the functional cointegration regressions strongly support the life cycle hypothesis on the demographic trend of the nominal short rate, via the impact of aggregate age impact on the real rate and inflation, respectively.

3 Functional Affine Arbitrage-free Term Structure Model with Aggregate Life Cycle Determinants

Although the single-equation functional analysis provides a consistent view on the trend driven mechanism of demographic age distribution on the nominal short rate, real rate and inflation, these results suffer from substantial parameter uncertainty due to limited data. For example, the S-shaped age impact function for the nominal short rate is not significant for the very young and the older population, resulting in uncertainty in the estimated trends, especially at the extreme levels of high and low yields. Similar pattern of estimation uncertainty is reported in Takamizawa (2008) when the short rate with nonlinear drift is inferred with single equation, and the paper shows usefulness of

exploring cross-section relations in the short end of the yield curve and expects more fundamental modeling utilizing the entire term structure.

In this section, a functional affine yield curve model is developed to fully explore the entire term structure and improve inference from the age impact function on one hand and use demographic trends to better explain yield curve dynamics on the other hand. The unified FATSM starts with a short rate composed of a global trend driven by the demographic age structure and local mean-reverting processes.

3.1 Short Rate Equation

First, denote the short rate $y_{t,1}$ of the term structure by i_t, i.e., $y_{t,1} = i_t$, which is composed of a long-term trend, i_t^*, and a cyclical component, $\tilde{\imath}_t$, such as $i_t = i_t^* + \tilde{\imath}_t$, and then assume that the time-varying trend, i_t^*, is driven by an aggregate determinant of the age distribution of population multiplied by its impact $g(s)$ for each age cohort s

$$i_t^* = \int_{\underline{S}}^{\bar{S}} f_t(s)g(s)ds, \tag{3.1}$$

where the age range is $s \in [\underline{S}, \bar{S}]$, $f_t(s)$ denotes the density function of the demographic distribution at time t, and $g(s)$ represents the age impact function for the short rate. In addition, the cyclical component is driven by short- and medium-term cyclical factors X_t with a typical affine representation

$$\tilde{\imath}_t = \delta_0 + \delta_1 X_t. \tag{3.2}$$

Next, the short rate equation can be summarized as follows:

$$y_{t,1} = \underbrace{\int_{\underline{S}}^{\bar{S}} f_t(s)g(s)ds}_{i_t^*} + \underbrace{\delta_0 + \delta_1 X_t}_{\tilde{\imath}_t}.$$

3.2 State Dynamics

We use f_t and X_t to denote state factors, the former being a slow-moving or long-term exogenous factor and the latter driving short- and medium-term fluctuations.

3.2.1 Slow-Moving Functional State of Age Density

The total population at time t is denoted by L_t, and the population of each age cohort on the age support $[s_{m-1}, s_m)$ is presented by $L_t^{s_m}$, born in the time interval $(t-s_m, t-s_m+1]$.

In practice, the age density can be approximated by the weight of the population of each age cohort in the M age intervals, $[0, s_1)$, $[s_1, s_2)$, ..., $[s_{m-1}, s_m)$, ..., $[s_{M-1}, \bar{S}]$:

$$w_t(s_m) = \int_{s_{m-1}}^{s_m} f_t(s)ds \approx L_t^{s_m}/L_t. \tag{3.3}$$

Suppose that the birth rate b_t is exogenous, such that the newly born cohort in the interval $(t-1, t]$ is $L_t^1 = b_t L_{t-1}$. Given a survival rate function $P_t^{s_m, s_{m+1}}$ for the population cohort $L_t^{s_m}$, the number of survivors of this cohort in the following period is $L_{t+1}^{s_{m+1}} = L_t^{s_m} P_t^{s_m, s_{m+1}}$. It is assumed that the survival rate function is stable over a long period under normal conditions without wars or natural disasters, which can be treated as a roughly constant $P^{s_m, s_{m+1}}$. These assumptions have two implications in practice. First, the survival rate can be approximated as a moving average over a past interval, say a few years. Second, the future population prediction in the medium to long-term, say 1 to 10 years, can be computed as follows:

$$E_t\left(L_{t+h}^{s_{m+h}}\right) = L_t^{s_m} \Pi_{j=1}^{h} P_{t+j-1}^{s_{m+j-1}, s_{m+j}},$$

which should be relatively accurate, based on $P^{s_{m+j-1}, s_{m+j}}$. Then, based on a reasonable projection of the birth rate, the age density for the short- to medium-term horizons can be predicted with little uncertainty using the projected population weights:

$$E_t\left[w_{t+h}(s_{m+h})\right] = E_t \int_{s_{m+h-1}}^{s_{m+h}} f_{t+h}(s)ds = E_t\left[L_{t+h}^{s_{m+h}}/L_{t+h}\right], \tag{3.4}$$

where $E_t L_{t+h} = E_t\left(\sum_{m=1}^{M} L_{t+h}^{s_m}\right)$.

3.2.2 Business Cycle Factors

As suggested by Diebold and Li (2006), the state dynamics of the cyclical mean-reverting process under the physical measurement can be modeled by a vector autoregression (VAR) of order 1, VAR(1), as follows:

$$X_t = \mu + \Phi X_{t-1} + v_t, \tag{3.5}$$

where $v_t \sim N(0, \Omega)$, and state dynamics under the risk-neutral measure can also be characterized by VAR(1) as, with $v_t^Q \sim N(0, \Omega)$,

$$X_t = \mu^Q + \Phi^Q X_{t-1} + v_t^Q. \tag{3.6}$$

3.3 Interest Rate Term Structure

A general form of yields also contains the two types of components of an affine form:

$$y_{t,n} = y^*_{t,n} + \tilde{y}_{t,n} = \int_{\underline{S}}^{\bar{S}} f_{t,n}(s)g(s)ds + a_n + b_n' X_t,$$

where each yield to maturity is composed of a time-varying long-term trend driven by the age distribution of the population, and a cyclical component $\tilde{y}_{t,n}$. Next, we show that the expectation hypothesis (EH) and the no-arbitrage assumption impose cross-equation restrictions on the functional factors $f_{t,n}(s)$ and the factor loadings a_n and b_n based on the short rate setting and state dynamics.

First, for the EH on the demographic trend $y^*_{t,n}$. As the population distribution is slow-moving and can be well predicted with little uncertainty under normal conditions, the EH is likely to suggest that $y^*_{t,n}$ is an expected average of the long-term component of the future short-rate i^*_{t+h}, which is driven by the future distribution f_{t+h}; that is $i^*_{t+h} = \int_{\underline{S}}^{\bar{S}} f_{t+h}(s)g(s)ds$, with $h = 0, \ldots, n-1$.

$$\begin{aligned} y^*_{t,n} &= \underbrace{\frac{1}{n} E_t \left[\sum_{h=0}^{n-1} i^*_{t+h} \right]}_{E.H.} = \frac{1}{n} E_t \left[\sum_{h=0}^{n-1} \int_{\underline{S}}^{\bar{S}} f_{t+h}(s)g(s)ds \right] = \int_{\underline{S}}^{\bar{S}} \left[\frac{1}{n} \sum_{h=0}^{n-1} E_t\{f_{t+h}(s)\} \right] g(s)ds \\ &= \int_{\underline{S}}^{\bar{S}} f_{t,n}(s)g(s)ds \end{aligned} \tag{3.7}$$

with

$$f_{t,n}(s) = \frac{1}{n} \sum_{h=0}^{n-1} E_t \left[f_{t+h}(s) \right], \tag{3.8}$$

where $f_{t,1}(s) \equiv f_t(s)$ and $f_{t+h}(s)$ can be approximated by the projected population weights as in (3.4). The implication is clear: the slow-moving age distribution of the population in long-term yields, $f_{t,n}(s)$, is an average of the expected age distribution evolving across the holding horizon.

Second, the cyclical component $\tilde{y}_{t,n}$ with the state dynamics given in (3.5) and (3.6) is written as

$$\tilde{y}_{t,n} = a_n + b_n' X_t,$$

where from $a_1 = \delta_0$ and $b_1 = \delta_1$ with short rate parameters as in (3.2), $a_n = -A_n/n$ and $b_n = -B_n/n$ can be derived from partial differential equations (PDEs) in the following

form (Ang and Piazzesi, 2003),

$$B'_{n+1} = B'_n \Phi^Q + B'_1, \tag{3.9}$$

and

$$A_{n+1} = A_n + B'_n \mu^Q + \frac{1}{2} B'_n \Omega B_n + A_1. \tag{3.10}$$

3.4 Statistical Representation

3.4.1 General Representation

In summary, the statistical representation of the FATSM is given by

$$y_{t,n} = \int_{\mathbb{S}}^{\bar{S}} f_{t,n}(s) g(s) ds + a_n + b'_n X_t + \epsilon_{t,n}, \quad \epsilon_{t,n} \sim N(0, \sigma^2_\epsilon), \tag{3.11}$$

which can also be regarded as a structural semiparametric model, where X_t follows a VAR(1) model as follows:

$$X_t = \mu + \Phi X_{t-1} + v_t, \quad v_t \sim N(0, \Omega)$$

with $f_{t,n}(s)$ defined in (3.8), and $a_n = -A_n/n$ and $b_n = -B_n/n$ defined in the PDEs in (3.9) and (3.10), respectively. Therefore, it can be seen that the yield is an affine form of the factors f_t and X_t with cross-equation restrictions under the EH and the no-arbitrage assumption. The slow-moving component is forward-looking, with current and future demographic structures having an effect via the age impact function $g(s)$.

3.4.2 Specific Representation of Cyclical Factors

The stationary no-arbitrage autoregressive part of the yields, $\tilde{y}_{t,n}$, can be described by any typical ATSM with specific factors X_t, such as latent factors or observed macroeconomic factors. To keep the parsimony in our semiparametric setting, we choose a simple affine arbitrage-free Nelson-Siegel (AFNS) model with the NS factor interpolation as follows:

$$B_n = \left(-n, -\frac{1 - e^{-\lambda n}}{\lambda}, n e^{-\lambda n} - \frac{1 - e^{-\lambda n}}{\lambda} \right)',$$

which corresponds to a risk-neutral transition matrix taking the following specific form

$$\Phi^Q = \begin{pmatrix} 1 & 0 & 0 \\ 0 & e^{-\lambda} & \lambda e^{-\lambda} \\ 0 & 0 & e^{-\lambda} \end{pmatrix}$$

as shown in Christensen et al. (2011) for a continuous-time setting and Hong et al. (2019) for a discrete-time case. The restriction that $a_1 = -A_1 = \delta_0 = 0$ can then be imposed for normalization. For parameter identification, we restrict $\mu^Q = (\mu_L^Q, 0, 0)'$ following Hong et al. (2019). Conditional on this basic AFNS model, we can compare our functional AFNS model(F-AFNS) with demographic trends in (3.11), the pure AFNS model, and an extended AFNS augmented by the single demographic index of the MY ratio (MY-AFNS). As has been discussed by Krippner (2015) and Christensen and Rudebusch (2019), the AFNS model can be viewed as a restricted version of the canonical Gaussian ATSM model. Therefore, our empirical framework can be easily generalized to the cases when choosing other specific ATSM models to capture the cyclical factors in yields.

4 Statistical Methodology

In this section, we first show how the two components of trends and autoregressive processes and their related parameters can be estimated in the classical framework, if they can be observed separately. Then, we discuss the joint estimation strategy in a Bayesian framework.

4.1 Nonparametric Trend Extraction Under the EH

In Section 2, we estimate the age impact function of the nominal short rate based on the age distribution of the population using a linear estimator in a single equation. Also, we exploit the rich information in the term structure for interest rates to robustly infer the common age impact function $g(s)$ under the EH from the structural equation of yields in (3.7). Similar to single equation regressions, the aforementioned Fourier flexible series approach is used to approximate the functional form as in (2.2). Then, the resulting approximation is given by

$$y_{t,n}^* = \int_{\underline{S}}^{\bar{S}} f_{t,n}(s) g(s) ds \approx \sum_{i=1}^{\kappa} \alpha_i \int_{\underline{S}}^{\bar{S}} f_{t,n}(s) \psi_i(s) ds, \tag{4.1}$$

which is similar to (2.3), except that we impose the EH restriction on the demographic distribution, as shown in (3.8). Again, based on the discretized age support with the weight of each cohort at time t and $t+h$, as shown in (3.3) and (3.4), the integral in (4.1) can be denoted by $z_{t,n,i}$ and approximated as

$$z_{t,n,i} \equiv \int_0^{\bar{S}} f_{t,n}(s)\psi_i(s)ds \approx \frac{1}{n}\sum_{h=0}^{n-1} E_t\left[\sum_{m=1}^{M} w_{t+h}(s_m)\psi_i(\bar{s}_m)\right] \tag{4.2}$$

with $\bar{s}_m = (s_{m-1} + s_m)/2$.

Given the above approximation, (4.1) can also be written in linear form as $y^*_{t,n} = \alpha' z_{t,n}$, where α is defined in (2.5), and similar to (2.5), $z_{t,n} = (z_{t,n,1} \cdots, z_{t,n,\kappa})'$ with $z_{t,n,i}$ defined in (4.2). For different yields to maturity, we have the common parameter vector α, so that a simultaneous equation regression is formed as $Y^*_t = Z'_t\alpha$, where Y^*_t is an $N \times 1$ vector of N observed yields and $Z_t = \left(z'_{t,n_1}, \cdots, z'_{t,n_N}\right)$ is a $\kappa \times N$ matrix. Then, with a sample of T observations for each yield-to-maturity, a compact linear form can be written as $Y^* = Z\,\alpha$, where $Y^* = \left(Y_1^{*'}, \cdots, Y_T^{*'}\right)'$ is an $NT \times 1$ vector and $Z = (Z_1, Z_2, \cdots, Z_T)'$ is an $NT \times \kappa$ matrix. Then the OLS estimator of α is given by

$$\widehat{\alpha} = (Z'Z)^{-1}Z'Y$$

with $Y = \left(Y_1', \cdots, Y_T'\right)'$ containing actual yield data.

Once $\widehat{\alpha}$ is obtained, its variance-covariance matrix can be estimated with the HAC procedure in Newey and West (1987) from the above simultaneous equation regression. Thus, we can obtain the age impact function and its variance-covariance matrix, similar to (2.6) and (2.7) as follows: for $1 \le m \le M$,

$$\widehat{g_\kappa}(\bar{s}_m) = \widehat{\alpha}'\Psi(\bar{s}_m) \quad \text{and} \quad \text{var}(\widehat{g_\kappa}) = \Psi'_\kappa \text{var}(\widehat{\alpha})\Psi_\kappa,$$

where Ψ_κ is defined in (2.7).

Again, we use the HCV and MHCV criteria to choose the best κ, similar to the idea described in Section 2.2. For any given block size h, the HCV criterion for structural estimation is given by

$$\text{HCV} = \frac{1}{T}\sum_{t=h}^{T-h} ||Y_t, Z'_t\widehat{\alpha}(t,h)||,$$

where $||A, B||$ denotes the Euclidean distance between the corresponding elements in the vectors A and B, and the estimator $\widehat{\alpha}(t,h)$ is obtained by removing the t-th observation and the h observations before and after the t-th observation in both Z and Y. Similarly,

$h = T/6$ is set as in Section 2.2. The MHCV criterion has the following form

$$\text{MHCV} = \text{HCV} + \frac{1}{T}\sum_{t=h}^{T-h}\sum_{s=1}^{T}||Y_s, Z_s'\widehat{\alpha}(t,h)|| + \frac{1}{T}\sum_{t=1}^{T}||Y_t, Z_t'\widehat{\alpha}||.$$

Then, the best κ can be chosen by minimizing the two CV criteria above.

4.2 Parametric Estimation of the Autoregressive Process

Given the observable $\tilde{y}_{t,n}$, the ATSM model has the following state space representation

$$\tilde{y}_{t,n} = a_n + b_n' X_t + \epsilon_{t,n}, \quad \epsilon_{t,n} \sim N(0, \sigma_\epsilon^2) \quad \text{and} \quad X_t = \mu + \Phi X_{t-1} + v_t, \quad v_t \sim N(0, \Omega),$$

where a_n and b_n are nonlinear functions of the underlying parameters, as shown in (3.9) and (3.10). Based on the distributional assumption of the error terms, the Gaussian model can be estimated using maximum likelihood estimation (MLE) with the Kalman filter (Ang and Piazzesi, 2003; Christensen et al., 2011). The nonlinearity of the factor loadings in the measurement equations makes MLE challenging both in terms of determining the global optimum and parameter uncertainty. To overcome this difficulty, we use the MCMC method, which has gained popularity in estimating such models, especially when hidden states are involved (Ang et al., 2011).

4.3 Joint Semiparametric Estimation Using the Bayesian Method

A simple way to jointly estimate the model is to use an iterative method with the two steps above until a certain threshold is reached. In the initial step, it is assumed that the yields are dominated by the long-term component with a zero mean cyclical component. Conditional on the extracted long-term part $y_{t,n}^*$, the remainder is modeled as $\tilde{y}_{t,n}$. However, consistency is not guaranteed in this procedure, because the simultaneous zero assumption of the cyclical components in the simultaneous equations is not compatible with the no-arbitrage condition. Therefore, we choose to jointly estimate the model with the MCMC approach described below.

The parameters to estimate are $\Theta = \left\{\alpha, \sigma_\epsilon^2, \mu, \Phi, \Omega, \mu_L^Q, \lambda\right\}$, and the latent variables to estimate are $X = \{X_1, \cdots, X_T\}$. For ease of illustration, the parameters are divided into four blocks: $\Theta_1 = \{\alpha, \sigma_\epsilon^2\}$, $\Theta_2 = \{\mu, \Phi\}$, $\Theta_3 = \{\Omega\}$, and $\Theta_4 = \left\{\mu_L^Q, \lambda\right\}$. The Metropolis-Hastings (MH) algorithm for Gibbs sampling used for the Bayesian estimation is closely related to that of Ang et al. (2007) and Hong et al. (2019). The detailed procedures for drawing the latent states and parameter blocks are as follows.

4.3.1 Drawing X_t

Based on the observed yield data $Y = (Y_1, \cdots, Y_T)$, the transformed linear regressors $Z = (Z_1, \cdots, Z_T)$, and the parameters derived from the last step, Θ^{d-1}, the forward filtering and backward smoothing algorithm as in Carter and Kohn (1994) is used to obtain the latent variables involved in X, denoted by X^d in the d-th draw.

4.3.2 Drawing μ and Φ

Given X^d, as X_t follows a VAR process in (3.5), μ and Φ can be obtained with standard Gibbs sampling with normal conjugate priors and posteriors. Note that the posteriors of μ and Φ conditional on Y, Z, X^d, and the other parameters are given by

$$\begin{aligned}
&P(\mu, \Phi | \Theta_1^{d-1}, \Theta_3^{d-1}, \Theta_4^{d-1}, Y, Z, X^d) \\
&\propto P(Y | \Theta_1^{d-1}, \Theta_3^{d-1}, \Theta_4^{d-1}, Z, X^d) P(X^d | \mu, \Phi, \Omega^{d-1}) P(\mu_0, \Phi_0) \propto P(X^d | \mu, \Phi, \Omega^{d-1}),
\end{aligned}$$

where $P(X^d | \mu, \Phi, \Omega^{d-1})$ is the likelihood function, which is normally distributed based on (3.5), and $P(\mu_0, \Phi_0)$ are the priors of μ and Φ. The validity of the passage from the first line to the second line is ensured by the PDEs in (3.9) and (3.10). As $\Theta_4 = \left\{\mu_L^Q, \lambda\right\}$, the bond price is independent of μ and Φ. Here, we use the non-informative prior (the so-called Jeffreys prior) on μ and Φ, so we only have to determine the likelihood functions of μ and Φ, which can be derived from the normal distribution. They are denoted by μ^d and Φ^d, respectively.

4.3.3 Drawing Ω

As Ω appears in the PDEs of (3.10) in a nonlinear fashion, there is no analytical expression of the conditional posterior distribution for Ω. Note that the posterior of Ω conditional on Y, Z, X^d, and the other parameters is given by

$$P(\Omega | \Theta_1^{d-1}, \Theta_2^d, \Theta_4^{d-1}, Y, Z, X^d) \propto P(Y | \Theta_1^{d-1}, \Theta_2^d, \Theta_4^{d-1}, \Omega, Z, X^d) P(X^d | \mu^d, \Phi^d, \Omega) P(\Omega_0),$$

where $P(\Omega_0)$ is the prior of Ω, which suggests an independent Metropolis draw. We draw the candidate Ω from the proposed density $q(\Omega) = P(X^d | \mu^d, \Phi^d, \Omega) P(\Omega_0)$, which is an inverse Wishart (IW) distribution if $P(\Omega_0)$ is specified as IW, so that $q(\Omega)$ is an IW natural conjugate. The proposal draw of Ω for the d-th draw is then accepted with the

probability β as follows:

$$\begin{aligned}\beta &= \min\left\{\frac{P(\Omega^d|\Theta_1^{d-1},\Theta_2^d,\Theta_4^{d-1},Y,Z,X^d)}{P(\Omega^{d-1}|\Theta_1^{d-1},\Theta_2^d,\Theta_4^{d-1},Y,Z,X^d)}\frac{q(\Omega^{d-1})}{q(\Omega^d)},1\right\}\\ &= \min\left\{\frac{P(Y|\Omega^d,\Theta_1^{d-1},\Theta_2^d,\Theta_4^{d-1},Z,X^d)}{P(Y|\Omega^{d-1},\Theta_1^{d-1},\Theta_2^d,\Theta_4^{d-1},Z,X^d)},1\right\}\end{aligned}$$

where the numerator and denominator of the last line are the likelihood functions, which are normally distributed based on the normality assumption for the measurement error $\epsilon_{t,n}$. Therefore, β is the likelihood ratio of the d-th draw to that of the $(d-1)$-th draw.

4.3.4 Drawing λ and μ_L^Q

Because both λ and μ_L^Q appear in the measurement equations in nonlinear form in the PDEs of (3.9) and (3.10), there are no analytical expressions of the conditional posterior distribution for these parameters. We draw λ and μ_L^Q one by one using a MH algorithm. We illustrate the sampling for λ below, and the sampling for μ_L^Q is similar. The posterior distribution of λ conditional on Y, Z, X^d, and the other parameters is given by

$$\begin{aligned}&P(\lambda|\Theta_1^{d-1},\Theta_2^d,\Theta_3^d,\mu_L^{Q^{d-1}},Y,Z,X^d)\\ &\propto P(Y|\Theta_1^{d-1},\Theta_2^d,\Theta_3^d,\mu_L^{Q^{d-1}},\lambda,Y,Z,X^d)P(\lambda_0)\propto P(Y|\Theta_1^{d-1},\Theta_2^d,\Theta_3^d,\mu_L^{Q^{d-1}},\lambda,Y,Z,X^d),\end{aligned}$$

where $P(\lambda_0)$ is the prior of λ. We use the non-informative prior, so that we only have the likelihood function to determine. λ enters the likelihood in a nonlinear way and λ is drew by using the random walk chain MH algorithm as $\lambda^d = \lambda^{d-1} + \tau_\lambda\eta$, where $\eta \sim N(0,1)$, and τ_λ is the scale parameter to control the acceptance rate. The acceptance probability of λ^d is given by

$$\begin{aligned}\beta &= \min\left\{\frac{P(\lambda^d|\Theta_1^{d-1},\Theta_2^d,\Theta_3^d,\mu_L^{Q^{d-1}},Y,Z,X^d)}{P(\lambda^{d-1}|\Theta_1^{d-1},\Theta_2^d,\Theta_3^d,\mu_L^{Q^{d-1}},Y,Z,X^d)}\frac{q(\lambda^{d-1}|\lambda^d)}{q(\lambda^d|\lambda^{d-1})},1\right\}\\ &= \min\left\{\frac{P(\lambda^d|\Theta_1^{d-1},\Theta_2^d,\Theta_3^d,\mu_L^{Q^{d-1}},Y,Z,X^d)}{P(\lambda^{d-1}|\Theta_1^{d-1},\Theta_2^d,\Theta_3^d,\mu_L^{Q^{d-1}},Y,Z,X^d)},1\right\}\\ &= \min\left\{\frac{P(Y|\Theta_1^{d-1},\Theta_2^d,\Theta_3^d,\mu_L^{Q^{d-1}},\lambda^d,Y,Z,X^d)}{P(Y|\Theta_1^{d-1},\Theta_2^d,\Theta_3^d,\mu_L^{Q^{d-1}},\lambda^{d-1},Y,Z,X^d)},1\right\}.\end{aligned}$$

4.3.5 Drawing α and σ_ϵ^2

Conditional on the d-th draw of the parameters in Θ_2^d, Θ_3^d, Θ_4^d, the latent variables X^d, the observed yield data Y, and the transformed linear regressors Z, the measurement

equation is reduced to a linear regression model. Thus, the conditional posterior of Θ_1 can be obtained using the Gibbs sampling procedure with the normal prior distribution and the inverse-Gamma prior distribution for α and σ_ϵ^2, respectively; see, for example, Chapter 8 of Koop (2003) for details. In practice, we set the variance-covariance matrix of the normal prior distribution for α to be the variance-covariance of the coefficients of the simultaneous equation regression, and let the prior mean be the OLS estimator for this regression.

5 Empirical Results

We run the MCMC procedure explained above for $220,000$ draws and keep the last $200,000$ draws after the initial $20,000$ burn-ins. Both for the single equation and simultaneous equation analysis, we choose $\kappa = 5$ according to the selection criteria. In the following, we report the estimation results and discuss their inference and forecast comparisons.

5.1 Parameter Estimation

Table 1 reports the parameter estimation results. The upper part includes the parameters of the measurement equations. The α values of the demographic distribution trend impact function are estimated significantly. The risk-neutral parameter λ implies that the curvature factor peaks around the maturity of six quarters, which is shorter than that of a traditional AFNS model with a higher value of λ. The lower part of Table 1 reports the state dynamic parameters of the NS factors in the physical VAR process. The diagonal elements in the autoregressive matrix are less persistent than the traditional estimates of an AFNS model without controlling for the slow-moving trend.

[Table 1: Parameter estimates based on the MCMC method]
[Table 2: Inefficiency factors of parameter posterior draws]

The convergence diagnostics based on the trace plots reported in Figure 6 and the inefficiency factors in Table 2 indicate convergence, although the inefficiency factors for the parameters in the measurement equations tend to be larger. The risk-neutral parameter μ_L^Q is the slowest to converge due to its nonlinearity when entering the measurement equations. However, with a large number of posterior draws $200,000$, convergence is achieved, as shown by the trace plots.

[Figure 6: Trace plots of the posterior draws]

Based on the estimation results, the goodness of fit of this model is shown in Table 3, which reports the descriptive statistics of the yield residuals. The standard deviations of the errors are mostly within 7 basis points (bps, 1 bp=0.01%), and the root mean squared errors (RMSE) or mean absolute errors (MAE) are on average only between 6 and 7 bps.

[Table 3: In-sample fit of the F-AFNS model: Residual statistics (bps)]

5.2 Impact Function, Trend, and Generation Impact Components

Figure 7 plots the estimated age impact function and implied trends in the joint model, where the solid lines are the median and the darker shaded area indicates the 95% confidence band. We also plot the corresponding single equation results using dashed lines with a lighter gray area indicating its 95% confidence interval. In comparison, when cross-maturity information in the term structure is used with higher efficiency, the joint estimation shrinks the confidence interval to a much smaller range. As a result, the left panel clearly shows that the previously non-significant impacts for the very young population before school years and the older population over 78 years of age become significantly negative and positive, respectively, and uncertainty about the implied trends is also reduced, especially between the mid-1970s and the mid-1980s around the turning point at the peak.

[Figure 7: Age impact functions and trends in the joint model versus single equation regressions]

To elaborate intuitively how the impact function works through each generation to drive the trend level of the short term interest rate, we demonstrate with Figure 8 and Figure 9 in two dimensions. In the time dimension, Figure 8 illustrates the life-long impact of the 1945 cohort in our sample. The upper panel shows its percentage share (density) in total population from 1952 to 2017 and projected share in dashed line from 2018 to 2027 with our calculation as explained in Section 3.2.1. The lower panel plots the estimated age impact function based on the joint model, starting from 1945 and age 0 for the 1945 cohort, and the red solid line indicates its impact component starting from 1952 in short term interest rate, as its share multiplied by the corresponding age impact along time and corresponding age. It shows that the impact component exhibits the S-shape of the impact function, but the amplitude tends to decrease as the share in the total population decreases.

[Figure 8: Population share of the 1945 cohort and its impact component in short rate]

In the age dimension at a particular time, Figure 9 shows how the trend level of the short rate is determined by the cross product of the population age density and the impact function, as defined by (3.1). Taking the situation in 2004 for example, Figure 9 plots the age density in the upper panel together with the impact function in the lower panel. Their cross product leads to a trend level of 3.83% for the short rate. To further demonstrates the generation impacts, we divide the population in our sample according to birth years into five major groups similar to Geanakoplos et al. (2004), with the three middle generations each spanning 20 years of birth dates. The five generations are labeled as pre boomers (born before 1945), baby boomers (1945-1964), generation X (1965-1984), echo boomers (1985-2004), and new millennium (since 2005). At 2004:Q4, the interest rate trend can be attributed to the aggregated impacts of the four generations born before 2005, which are indicated by dashed line segments for corresponding generations, as -4.37%, -7.98%, 12.27%, and 3.81% for pre boomers, baby boomers, generation X, and echo boomers, respectively. It can be seen that the baby boomers contribute a substantial negative component as they entered into a life stage of yielding negative impact on the interest rate, especially on real rate. The pre boomers are the most aged and also contribute negatively. Although the impact function has a positive tale at the upper end, those aged above 78 has a diminishing weight and thus a minor impact.

[Figure 9: Age distribution of the population at 2004:Q4 and age impact function]

From a perspective of generation impact, our results help understanding the large swing of the yield trends in relation to demographic age structure. We compute the impact components contributed by the five generations to the short rate trend in the whole sample and plot them in Figure 10. It can be seen that each generation exerts a similar S-shaped impact along their life time, but the impact of the baby boomers is amplified by their bulky weight, thus resulting in a short rate trend mirroring much of the boomer's cycle. Figure 10 also plots the projected impact of each generation from 2018 to 2027 in dashed lines, which predict a persistently flattened short rate trend merely above zero. Although the baby boomer's age impact function turns upward during this period, due to its diminishing weight as aged population, their aggregated impact no longer dominates.

[Figure 10: The short rate trend and impact components of different generations]

Our results show that the joint model can fully utilize the cross-section information within both the population density and the yield curve to make more in-depth analysis

on the relationship between the full range of demographic structure and the trend in interest rates. The results yield two insights: first, demographic shocks exert life-long impacts on interest rates which only die out after decades, thus explaining the persistence of yields; second, the impact of demographic shocks varies along the life cycle and the aggregated impacts of historical demographic shocks determine aggregately the level of trend in interest rates, thus explaining the pattern of yield trends.

5.3 Term Structure Decomposition

The trends in each yield of maturity form a demographic term structure, as plotted in Figure 11. Figure 11 clearly shows how the expected movement in the age distribution of the population actually shapes the slow-moving term structure at different stages: upward sloping in the 1960s through the mid-1970s due to the high birth rate of baby boomers and their increasing impact on interest rates when they were young, downward sloping from the 1980s for more than three decades as baby boomers matured and aged, and flat during transitional periods such as the second half of the 1970s and recent years. The term spread determined by the expected demographic trend can reach up to 70 bps for the upward trend with a positive slope and around 100 bps for the downward track with a negative slope.

[Figure 11: Demographic trend term structure of interest rates]

Conditional on the slow-moving demographic-trend term structure, there is a stationary term structure in the yield curve driven by autoregressive process, as plotted in Figure 12. Nonstationarity are rejected by ADF test for all these cyclical components of different maturities, which again validates the cointegration relationship between the functional factors of the demographic age distribution and the yield curve. From the statistics in Table 4, which compares the actual term structure and its two components, we can see that the average term spread of the 5-year yield minus the 3-month yield in this cyclical term structure is 1.253%, 16.6 bps higher than the yield difference, and the variance of cyclical yields is about 50% less than that of all yields. The higher term spread in the cyclical components implies that risk premia are more important for long-term yields during the sample period, after controlling for the trend structure.

[Figure 12: Stationary term structure of interest rates]
[Table 4: Statistics of the decomposed term structure (%)]

To see the model-implied dynamics of risk premia illustrated in Figure 13, the 5-year yield is decomposed into expectation and risk premia, and the former contains demographic expectation (trend) and expectation of the cyclical component (expected average of cyclical short-term yields in future horizons). It can be seen that now the expectation term dominates in the 5-year yield. The expected yield almost always decreases during a recession, and the risk premium fluctuates more than the expectation term. In comparison, if the 5-year risk premium is computed from an AFNS model without controlling for the demographic trend, the risk premium contributes more in the upward trend period before the late 1970s and matters less in the downward trend period, especially in the last 10 years of the sample.

[Figure 13: Decomposition of the 5-year yield]

Taking the model-implied risk premia and computing their correlation with real activity indicators, such as the industrial production (IP) growth and real consumption growth, Table 5 shows that the risk premia in our model are negatively correlated with these macroeconomic variables with a counter cyclical feature as predicted by theory. The risk premia in an AFNS model do not exhibit such a feature.

[Table 5: Correlation between risk premia and real activities]

5.4 Forecast Comparisons

We compare the out-of-sample forecasting performance of our model with a few alternatives, including a discrete-time AFNS as in Christensen et al. (2011) and Hong et al. (2019), a dynamic Nelson-Siegel model (DNS) without the no-arbitrage assumption as in Diebold and Li (2006), the single index demographic trend no-arbitrage model (MY-AFNS) similar to that in Favero et al. (2016), and a random walk model without drift.

We use recursive window estimation, with the first window starting from 1952:Q2 to 1999:Q4 for 1-, 4-, 8-, 12-, 16-, and 20-quarter ahead forecasts, and move one quarter at a time with an expanding window for the next set of 1- to 20-quarter ahead forecasts, until we reach the end of the sample. The root mean squared forecast error (RMSFE) results are reported in Figure 14, from which it can be seen that no alternative models perform better than our F-AFNS model for 4- to 20-quarter ahead forecasts.

[Figure 14: Forecast comparisons based on the RMSFE]

Finally, the error terms in the alternative models increase with the forecast horizons, but the errors in the F-AFNS model exhibit a slightly hump-shaped pattern, increasing up

to the 12-quarter horizon and decreasing afterward, such that the errors in the 20-quarter horizon stabilize within 120 bps across maturities. This non-diverging pattern of errors along the forecast horizons demonstrates unbiased trend forecasts.

6 Conclusion

We propose a unified functional affine term structure modeling framework, called the FATSM model, to incorporate a long-term trend driven by the age distribution of the population through a life cycle impact function. The model explains the trend behavior of interest rates with a theoretical basis and empirical power. First, our model links the time-varying long-term trend of interest rates with fundamental and permanent demographic shocks which exert a life cycle impact and take a life time to die out. Second, the information in the term structure is used efficiently to infer the age impact function with parameters tightening, and the resulting age impact function shows a life cycle pattern consistent with the impact of real rate and inflation trends in a Fisher equation framework. Third, the strong identification of a slow-moving trend as the integrated effect of the evolution of the age distribution helps to decompose the interest rate term structure into a persistent demographic-driven term structure and a stationary one featuring business cycle fluctuation.

Applying the proposed model to U.S. data from 1950 to the recent period, we find remarkable evidence of the consistency of our model with the yield data. After removing the demographic-driven cointegrated trends, the remaining term structure is stationary and the implied risk premia are counter cyclical. The out-of-sample performance of the model is better than that of alternatives models for 4- to 20-quarter ahead yield forecasts across maturities.

Finally, the extension of the proposed model to a joint framework with inflation-protected bond yields may help to better understand the age impact functions for inflation and real rate trends over the life cycle, and is left for future research.

References

Abel, A. B. (2003). The effects of a baby boom on stock prices and capital accumulation in the presence of social security. *Econometrica 71*(2), 551–578.

Aksoy, Y., H. S. Basso, R. P. Smith, and T. Grasl (2019). Demographic structure and macroeconomic trends. *American Economic Journal: Macroeconomics 11*(1), 193–222.

Andrews, D. W. (1991). Asymptotic normality of series estimators for nonparametric and semiparametric regression models. *Econometrica 59*(1), 307–345.

Ang, A. and G. Bekaert (2002). Regime switches in interest rates. *Journal of Business & Economic Statistics 20*(2), 163–182.

Ang, A., J. Boivin, S. Dong, and R. Loo-Kung (2011). Monetary policy shifts and the term structure. *Review of Economic Studies 78*(2), 429–457.

Ang, A., S. Dong, and M. Piazzesi (2007). No-arbitrage Taylor rules. Technical report, National Bureau of Economic Research.

Ang, A. and A. Maddaloni (2005). Do demographic changes affect risk premiums? Evidence from international data. *Journal of Business 78*(1), 341–380.

Ang, A. and M. Piazzesi (2003). A no-arbitrage vector autoregression of term structure dynamics with macroeconomic and latent variables. *Journal of Monetary Economics 50*(4), 745–787.

Bakshi, G. S. and Z. Chen (1994). Baby boom, population aging, and capital markets. *Journal of Business 67*(1), 165–202.

Balduzzi, P., S. R. Das, and S. Foresi (1998). The central tendency: A second factor in bond yields. *Review of Economics and Statistics 80*(1), 62–72.

Bansal, R. and H. Zhou (2002). Term structure of interest rates with regime shifts. *Journal of Finance 57*(5), 1997–2043.

Bauer, M. D. and G. D. Rudebusch (2020). Interest rates under falling stars. *American Economic Review 110*(5), 1316–54.

Bauer, M. D., G. D. Rudebusch, and J. C. Wu (2012). Correcting estimation bias in dynamic term structure models. *Journal of Business & Economic Statistics 30*(3), 454–467.

Bloom, D. E., D. Canning, and B. Graham (2003). Longevity and life-cycle savings. *Scandinavian Journal of Economics 105*(3), 319–338.

Bowsher, C. G. and R. Meeks (2008). The dynamics of economic functions: Modeling and forecasting the yield curve. *Journal of the American Statistical Association 103*(484), 1419–1437.

Browning, M. and M. Ejrnæs (2009). Consumption and children. *Review of Economics and Statistics 91*(1), 93–111.

Bullard, J., C. Garriga, C. J. Waller, et al. (2012). Demographics, redistribution, and optimal inflation. *Federal Reserve Bank of St. Louis Review 94*(6), 419–39.

Burman, P., E. Chow, and D. Nolan (1994). A cross-validatory method for dependent data. *Biometrika 81*(2), 351–358.

Carter, C. K. and R. Kohn (1994). On gibbs sampling for state space models. *Biometrika 81*(3), 541–553.

Carvalho, C., A. Ferrero, and F. Nechio (2016). Demographics and real interest rates: Inspecting the mechanism. *European Economic Review 88*, 208–226.

Chen, Y. and L. Niu (2014). Adaptive dynamic Nelson–Siegel term structure model with applications. *Journal of Econometrics 180*(1), 98–115.

Chib, S. and B. Ergashev (2009). Analysis of multifactor affine yield curve models. *Journal of the American Statistical Association 104*(488), 1324–1337.

Christensen, J. H., F. X. Diebold, and G. D. Rudebusch (2011). The affine arbitrage-free class of Nelson–Siegel term structure models. *Journal of Econometrics 164*(1), 4–20.

Christensen, J. H. and G. D. Rudebusch (2019). A new normal for interest rates? Evidence from inflation-indexed debt. *Review of Economics and Statistics 101*(5), 933–949.

Cieslak, A. and P. Povala (2015). Expected returns in treasury bonds. *Review of Financial Studies 28*(10), 2859–2901.

Cocco, J. F. and F. J. Gomes (2012). Longevity risk, retirement savings, and financial innovation. *Journal of Financial Economics 103*(3), 507–529.

Cooley, T. and E. Henriksen (2018). The demographic deficit. *Journal of Monetary Economics 93*, 45–62.

Cox, J. C., J. E. Ingersoll, and S. A. Ross (1985). A theory of the term structure of interest rates. *Econometrica 53*(2), 385–407.

Del Negro, M., D. Giannone, M. P. Giannoni, and A. Tambalotti (2019). Global trends in interest rates. *Journal of International Economics 118*(1), 248–262.

DellaVigna, S. and J. M. Pollet (2007). Demographics and industry returns. *American Economic Review 97*(5), 1667–1702.

Diebold, F. X. and C. Li (2006). Forecasting the term structure of government bond yields. *Journal of Econometrics 130*(2), 337–364.

Duffee, G. R. (2018). Expected inflation and other determinants of treasury yields. *Journal of Finance 73*(5), 2139–2180.

Eggertsson, G. B., N. R. Mehrotra, and J. A. Robbins (2019). A model of secular stagnation: Theory and quantitative evaluation. *American Economic Journal: Macroeconomics 11*(1), 1–48.

Fair, R. C. and K. M. Dominguez (1991). Effects of the changing U.S. age distribution on macroeconomic equations. *American Economic Review 81*(5), 1276–1294.

Fama, E. F. (2006). The behavior of interest rates. *Review of Financial Studies 19*(2), 359–379.

Favero, C. A., A. E. Gozluklu, and A. Tamoni (2011). Demographic trends, the dividend-price ratio, and the predictability of long-run stock market returns. *Journal of Financial and Quantitative Analysis 46*(5), 1493–1520.

Favero, C. A., A. E. Gozluklu, and H. Yang (2016). Demographics and the behavior of interest rates. *IMF Economic Review 64*(4), 732–776.

Gagnon, E., B. K. Johannsen, and D. López-Salido (2021). Understanding the new normal: the role of demographics. *IMF Economic Review 69*(2), 357–390.

Geanakoplos, J., M. Magill, and M. Quinzii (2004). Demography and the long-run predictability of the stock market. *Brookings Papers on Economic Activity 2004*(1), 241–325.

Ghysels, E. and S. Ng (1998). A semiparametric factor model of interest rates and tests of the affine term structure. *Review of Economics and Statistics 80*(4), 535–548.

Goliński, A. and P. Zaffaroni (2016). Long memory affine term structure models. *Journal of Econometrics 191*(1), 33–56.

Goodhart, C. and M. Pradhan (2020). *The great demographic reversal: Ageing societies, waning inequality, and an inflation revival*. Springer Nature.

Goyal, A. (2004). Demographics, stock market flows, and stock returns. *Journal of Financial and Quantitative Analysis 39*(1), 115–142.

Gozluklu, A. and A. Morin (2019). Stock vs. bond yields and demographic fluctuations. *Journal of Banking & Finance 109*, 105683.

Härdle, W. K. and P. Majer (2016). Yield curve modeling and forecasting using semi-parametric factor dynamics. *European Journal of Finance 22*(12), 1109–1129.

Higgins, M. (1998). Demography, national savings, and international capital flows. *International Economic Review 39*(2), 343–369.

Hong, Z., L. Niu, and G. Zeng (2019). US and Chinese yield curve responses to RMB exchange rate policy shocks. *China Finance Review International 9*(3), 360–385.

Hubener, A., R. Maurer, and O. S. Mitchell (2016). How family status and social security claiming options shape optimal life cycle portfolios. *Review of Financial Studies 29*(4), 937–978.

Juselius, M. and E. Takáts (2021). Inflation and demography through time. *Journal of Economic Dynamics and Control 128*, 104136.

Katagiri, M., H. Konishi, and K. Ueda (2020). Aging and deflation from a fiscal perspective. *Journal of Monetary Economics 111*(1), 1–15.

Koop, G. (2003). *Bayesian Econometrics*. John Wiley & Sons, New York.

Kowala, D. R., D. S. Mattesona, and D. Ruppert (2017). A Bayesian multivariate functional dynamic linear model. *Journal of the American Statistical Association 112*(518), 733–744.

Krippner, L. (2015). A theoretical foundation for the Nelson–Siegel class of yield curve models. *Journal of Applied Econometrics 30*(1), 97–118.

Krueger, D. and A. Ludwig (2007). On the consequences of demographic change for rates of returns to capital, and the distribution of wealth and welfare. *Journal of Monetary Economics 54*(1), 49–87.

Lindh, T. and B. Malmberg (2000). Can age structure forecast inflation trends? *Journal of Economics and Business 52*(1-2), 31–49.

Love, D. A. (2010). The effects of marital status and children on savings and portfolio choice. *Review of Financial Studies 23*(1), 385–432.

Lunsford, K. G. and K. D. West (2019). Some evidence on secular drivers of us safe real rates. *American Economic Journal: Macroeconomics 11*(4), 113–39.

McMillan, H. M. and J. B. Baesel (1990). The macroeconomic impact of the baby boom generation. *Journal of Macroeconomics 12*(2), 167–195.

Modigliani, F. (1966). The life cycle hypothesis of saving, the demand for wealth and the supply of capital. *Social Research*, 160–217.

Newey, W. K. and K. D. West (1987). A simple, positive semi-definite, heteroskedasticity and autocorrelation. *Econometrica 55*(3), 703–708.

Papetti, A. (2021). Demographics and the natural real interest rate: historical and projected paths for the euro area. *Journal of Economic Dynamics and Control*, 104209.

Park, C. (2010). How does changing age distribution impact stock prices? A nonparametric approach. *Journal of Applied Econometrics 25*(7), 1155–1178.

Park, J. Y., K. Shin, and Y.-J. Whang (2010). A semiparametric cointegrating regression: Investigating the effects of age distributions on consumption and saving. *Journal of Econometrics 157*(1), 165–178.

Poterba, J. M. (2001). Demographic structure and asset returns. *Review of Economics and Statistics 83*(4), 565–584.

Racine, J. (1997). Feasible cross-validatory model selection for general stationary processes. *Journal of Applied Econometrics 12*(2), 169–179.

Ramsay, J. O. and B. W. Silverman (1997). *Functional Data Analysis*. Springer, New York.

Takamizawa, H. (2008). Is nonlinear drift implied by the short end of the term structure? *The Review of Financial Studies 21*(1), 311–346.

Vasicek, O. (1977). An equilibrium characterization of the term structure. *Journal of Financial Economics 5*(2), 177–188.

Zantedeschi, D., P. Damien, and N. Polson (2011). Predictive macro-finance with dynamic partition models. *Journal of the American Statistical Association 106*(494), 427–439.

Zhang, J., J. Zhang, and R. Lee (2003). Rising longevity, education, savings, and growth. *Journal of Development Economics 70*(1), 83–101.

Figures and Tables

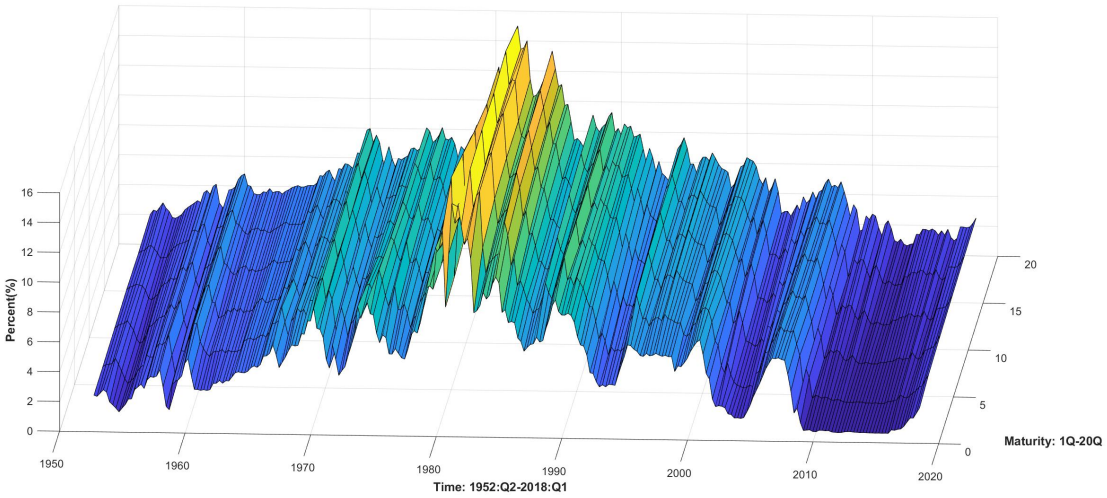

Figure 1. U.S. Treasury yield curve from 1952:Q2 to 2018:Q1

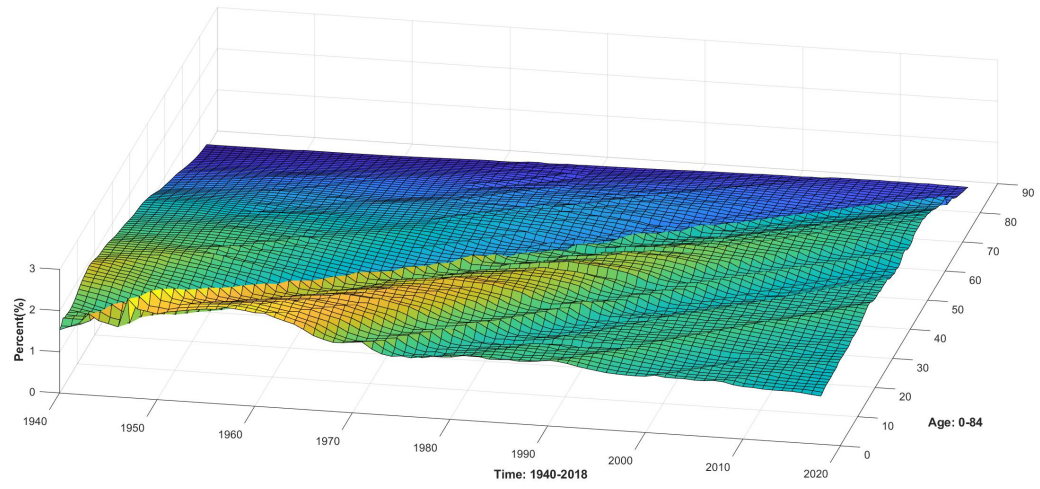

Figure 2. Dynamics of the age distribution of the U.S. population

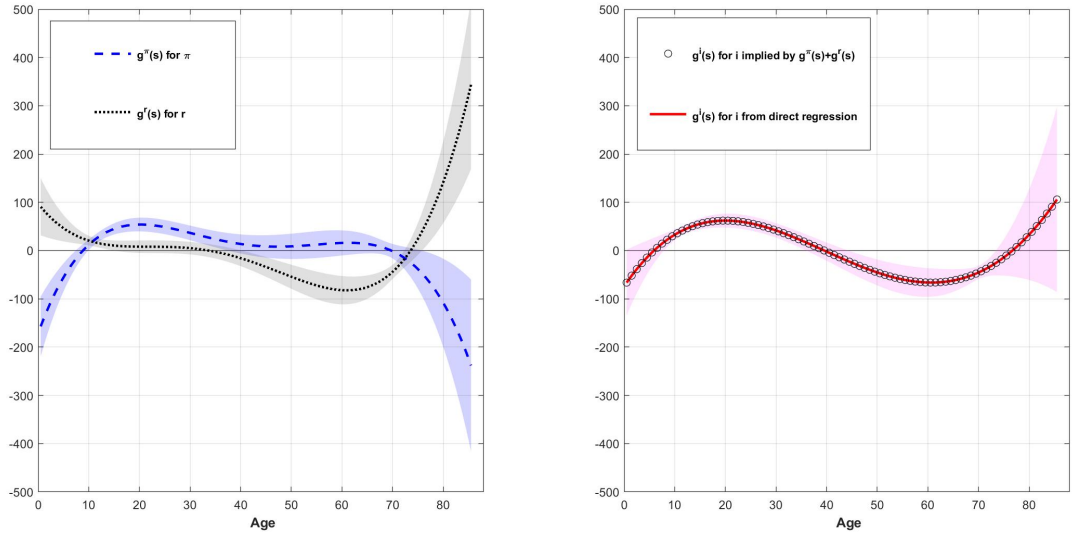

Note: 1) The left panel shows the age impact functions estimated from single equation regressions for inflation (dashed line) and the real rate (dotted line); 2) The right panel shows the age impact function for the nominal short rate, where the circle indicates the implied impact functions as a sum of impact functions for real rate and inflation, and the solid line indicates the impact function estimated directly from the regression with nominal short rate; 3) In both panels, the shaded areas indicate the 95% confidence interval of the estimated impacts.

Figure 3. Age impact functions of single equation regressions

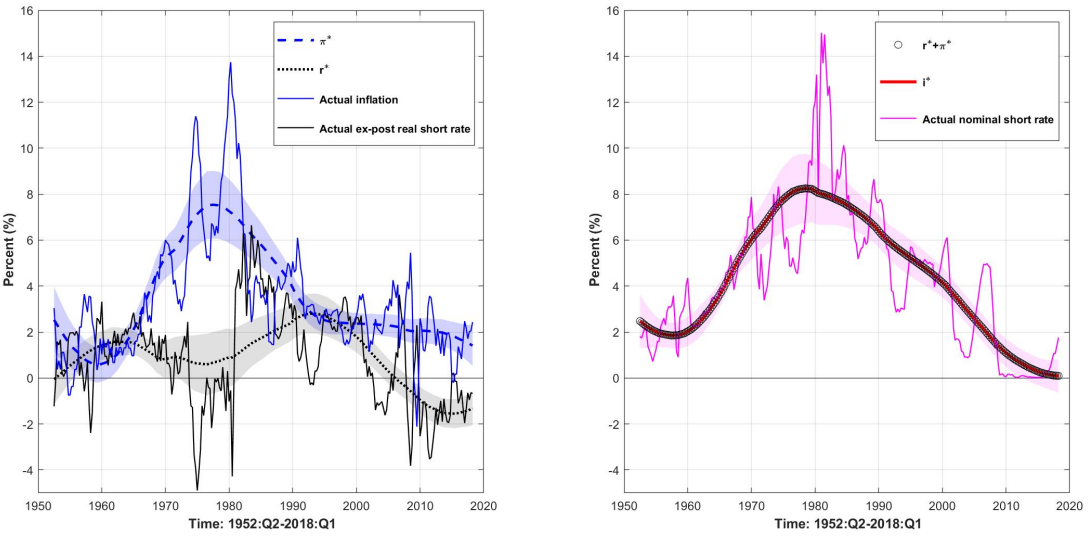

Note: 1) The left panel shows the trends estimated from single equation regressions for inflation (dashed line) and the real rate (dotted line); 2) The right panel shows the trend for the nominal short rate, where the circle indicates the implied trend as a sum of trends for real rate and inflation, and the solid line indicates the trend estimated directly from the regression with nominal short rate; 3) In both panels, the shaded areas indicate the 95% confidence interval of the estimated impact function.

Figure 4. Demographic trends of single equation regressions

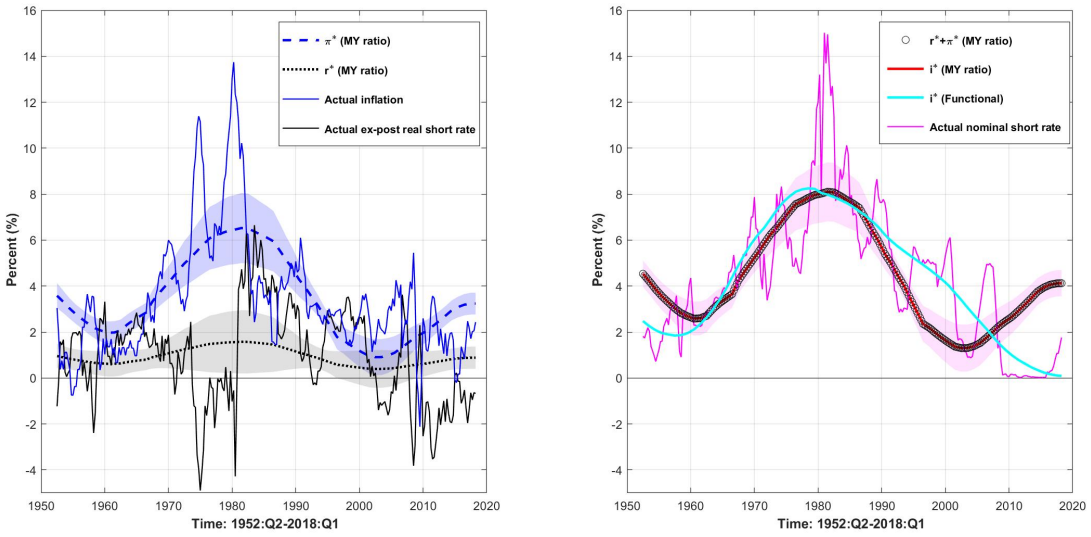

Note: 1) The left panel shows the trends estimated from inflation (dashed line) and the real rate (dotted line) regression on a constant and MY ratio, respectively ; 2) The right panel shows the trend for the nominal short rate, where the circle indicates the implied trend as a sum of trends for real rate and inflation from the left panel, and the red solid line indicates the trend estimated directly from the regression with nominal short rate, while the cyan solid line indicates the nominal short rate trend estimated from the functional regression as shown in Figure 4; 3) In both panels, the shaded areas indicate the 95% confidence interval of the estimated impact function.

Figure 5. Trends explained by the MY ratio

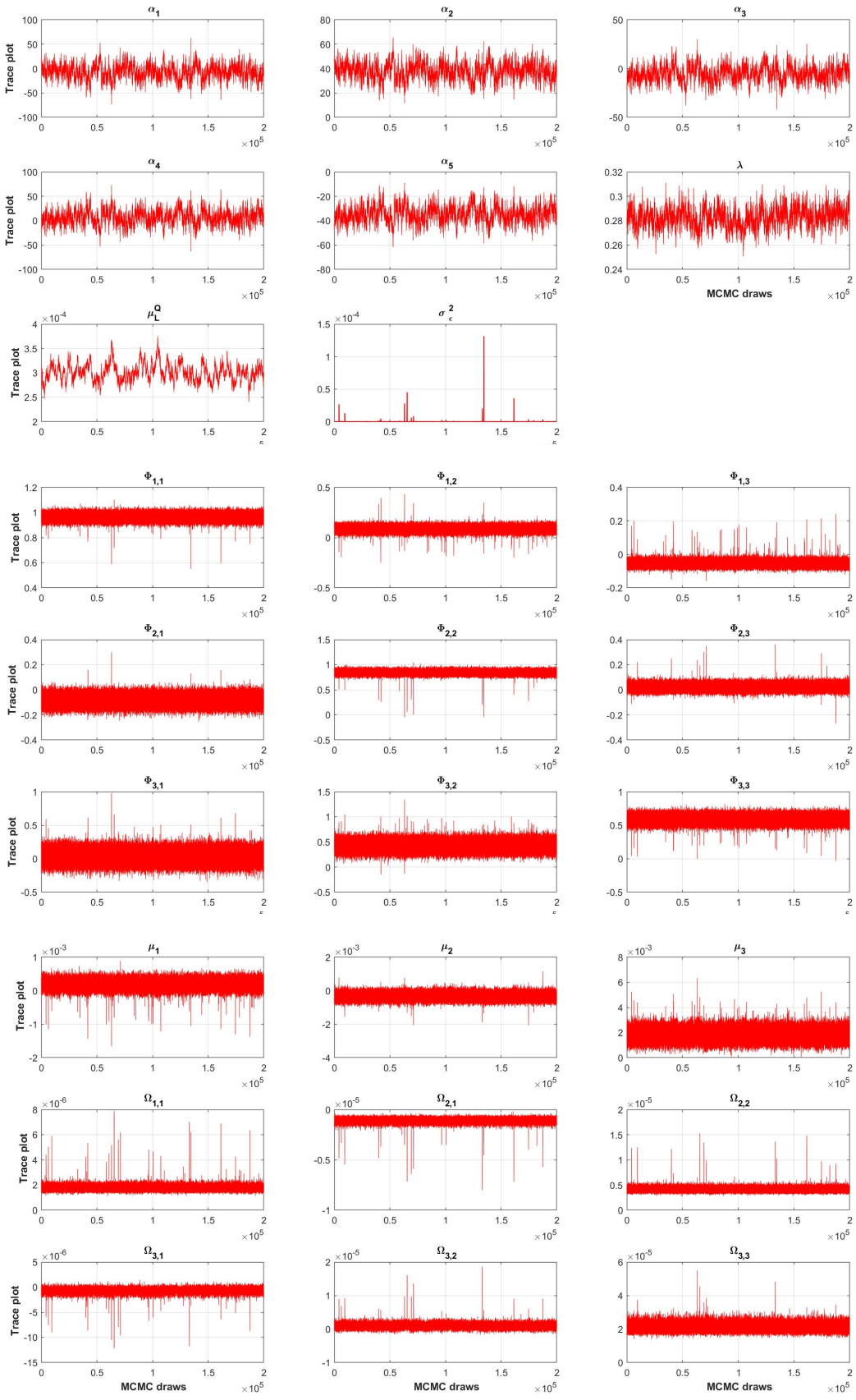

Figure 6. Trace plots of the posterior draws

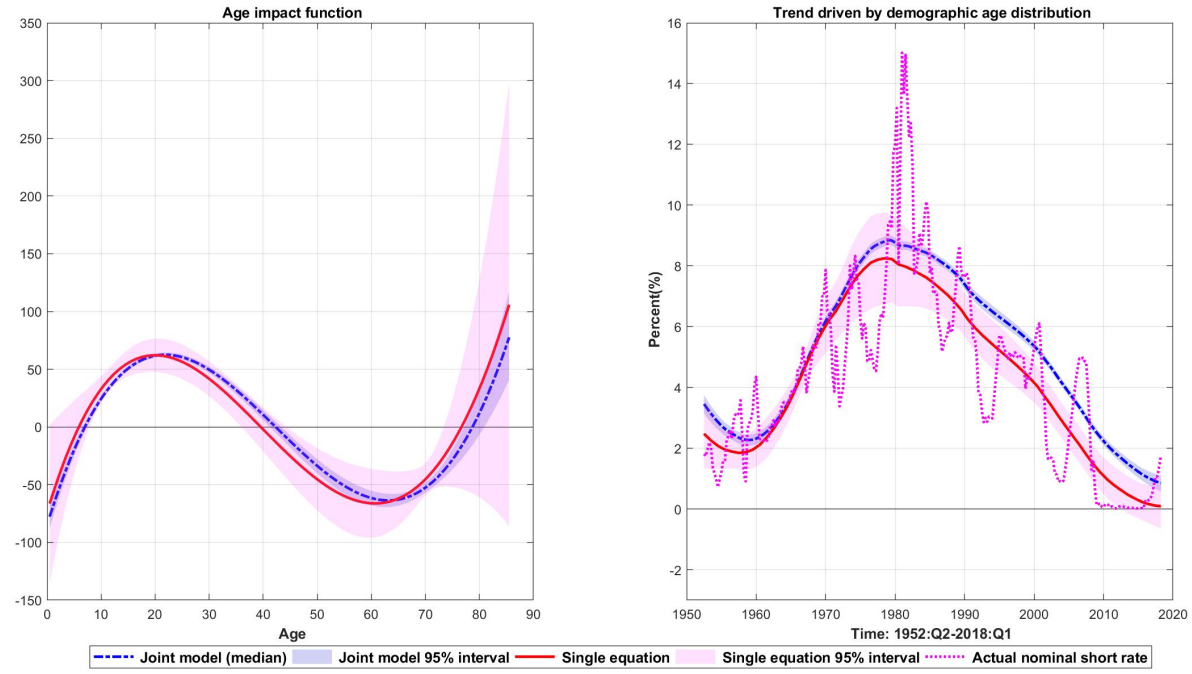

Figure 7. Age impact functions and trends in the joint model versus single equation regressions

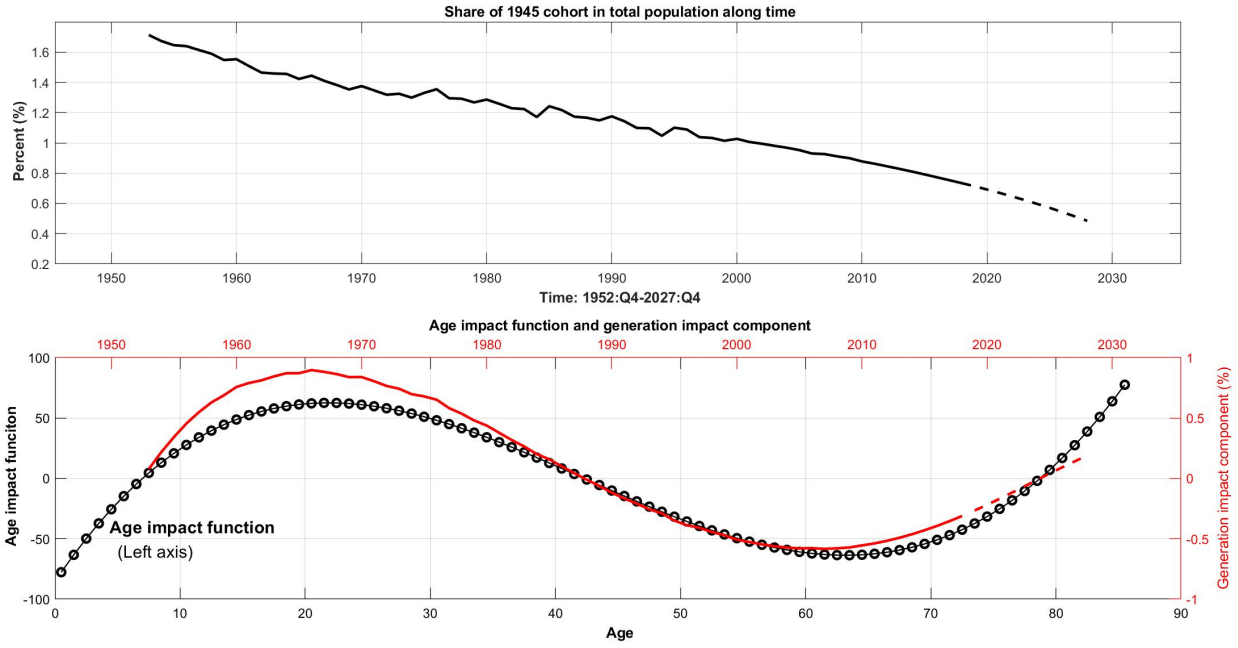

Note: The upper panel shows the percentage share (density) of the 1945 cohort in total population from 1952 to 2017 and its projected share in dashed line from 2018 to 2027; The lower panel plots the age impact function starting from 1945 and age 0 for the 1945 cohort, and the red solid line indicates its impact component starting from 1952 in short term interest rate.

Figure 8. Population share of the 1945 cohort and its impact component in short rate

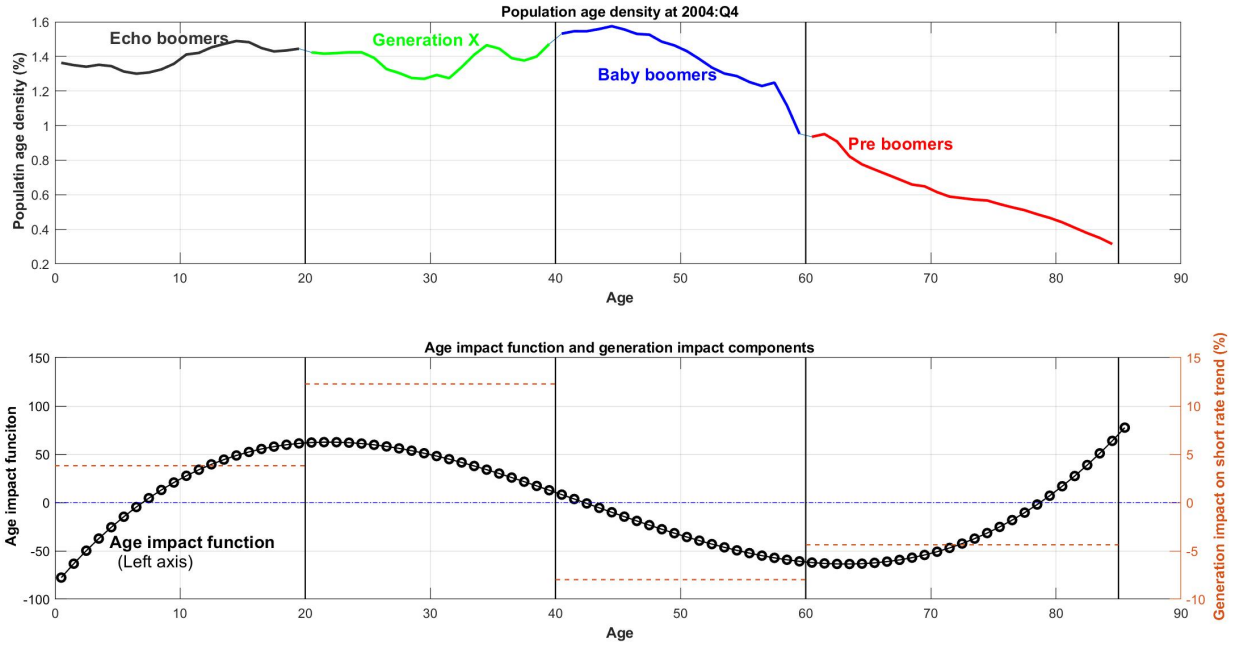

Note: This figure shows the age impact function (left axis of lower subplot) and the population age distribution at 2004:Q4 labeled with four generations. The aggregated impact of each generation on the trend level of short rate is indicated by a dashed line segment measured by percentage (right axis of lower subplot).

Figure 9. Age distribution of the population at 2004:Q4 and age impact function

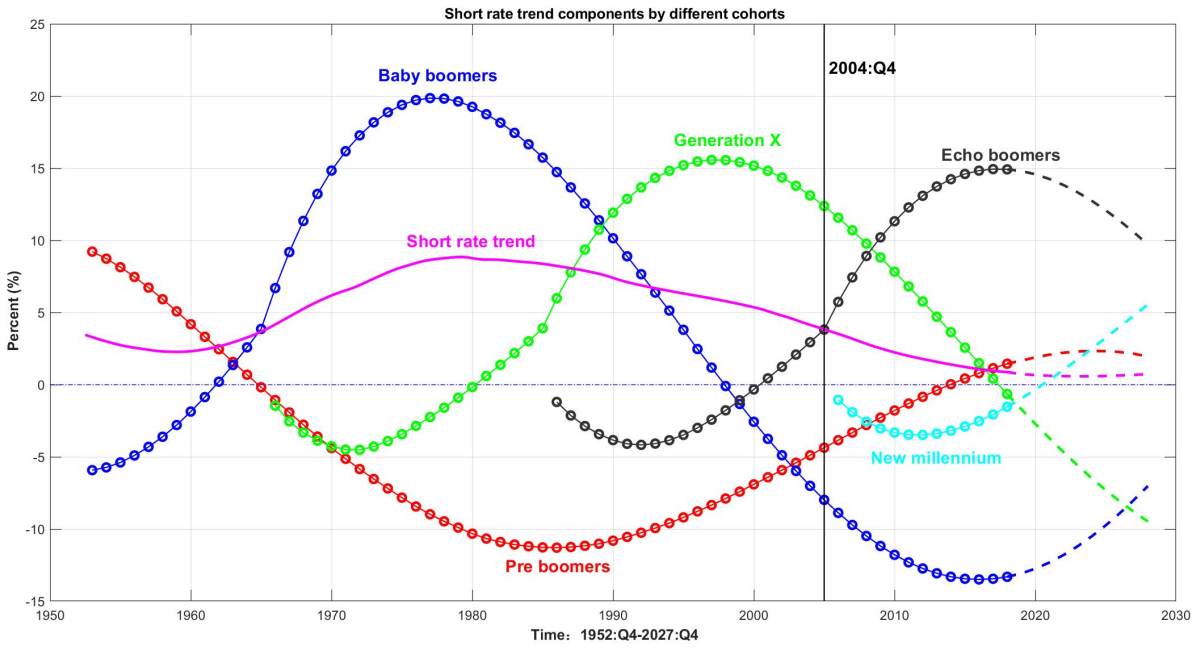

Note: This figure shows the short rate trend in solid line and the impact components of five generations in circled lines along time. The generation component is computed as the aggregated age impacts of all cohorts within a generation. The dashed lines from 2018 to 2027 are projections based on the joint model.

Figure 10. The short rate trend and impact components of different generations

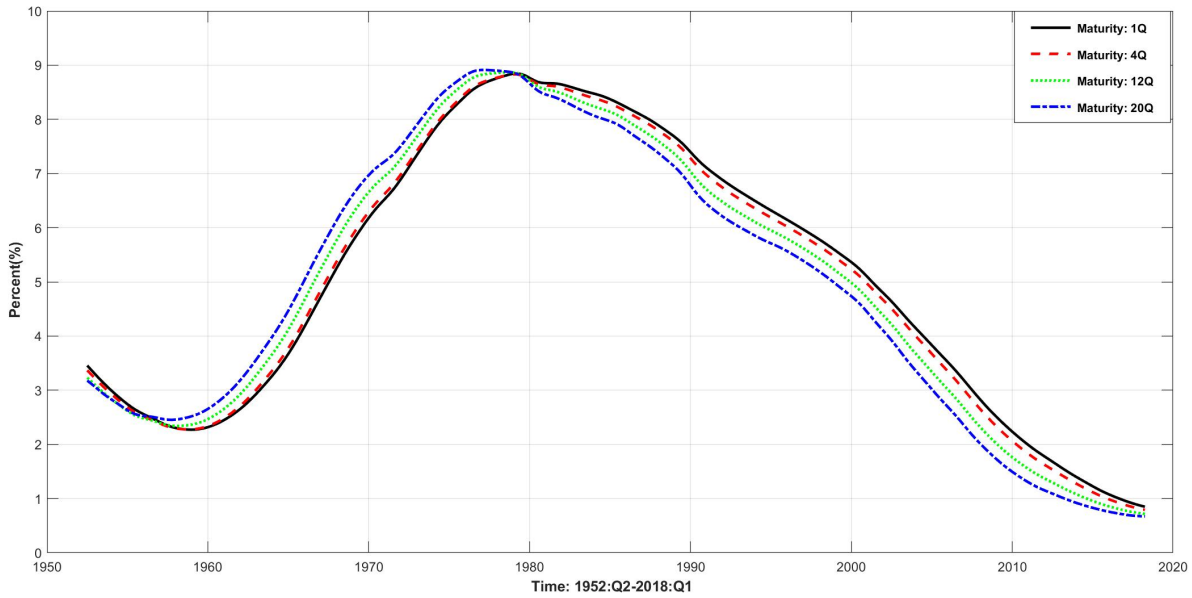

Note: This figure shows the slow-moving trends of interest rates of 1 quarter (1Q) to 20 quarters (20Q) as explained by the integrated effect of the evolution of the US population of different age cohorts within those related bond holding terms.

Figure 11. Demographic term structure of interest rates

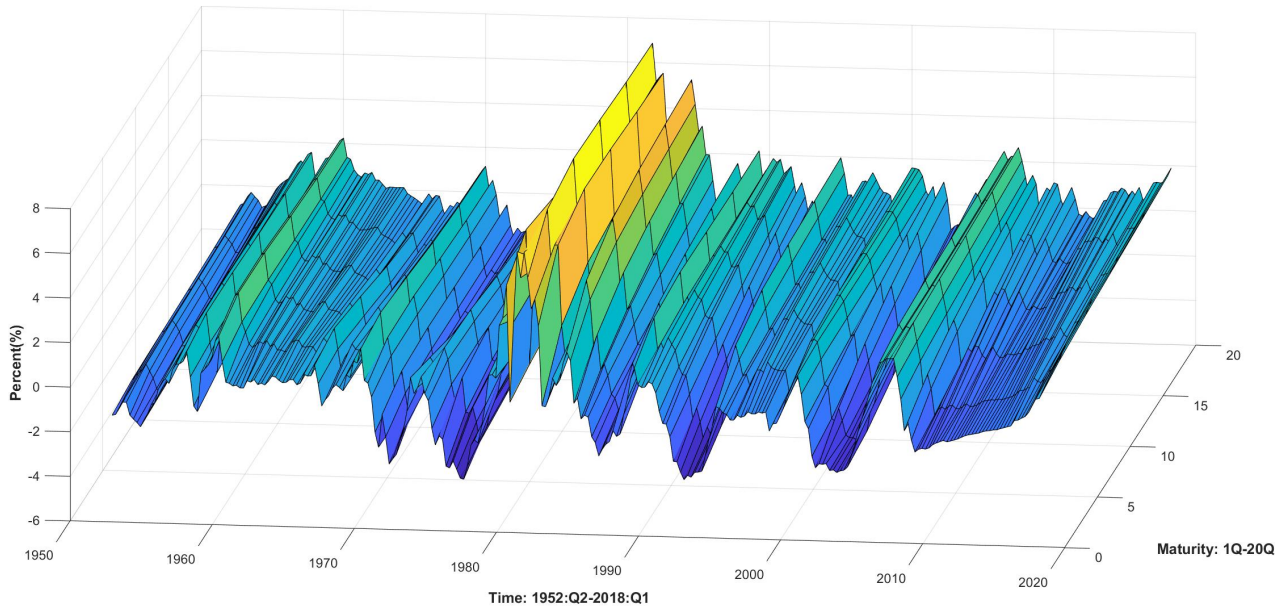

Note: This figure shows the cyclical components of US interest rate term structure from 1 quarter (1Q) to 20 quarters (20Q), after excluding demographic-driven trends.

Figure 12. Cyclical term structure of interest rates

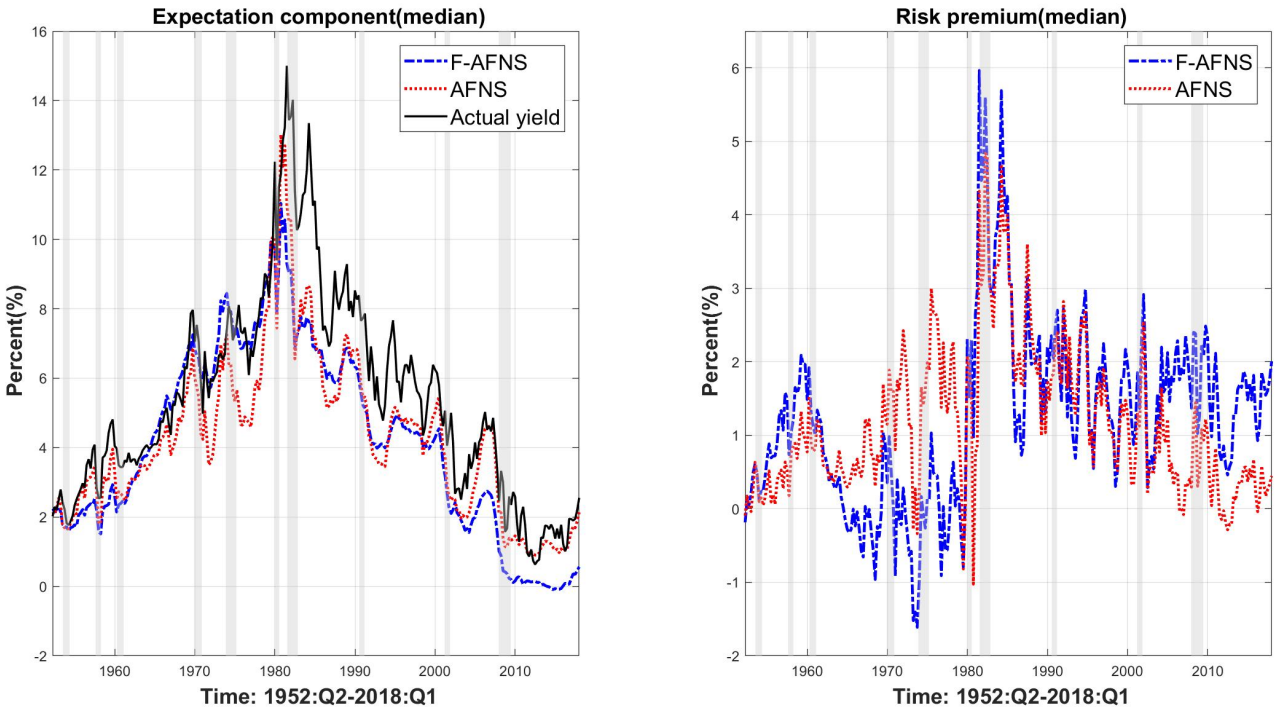

Note: This figure compares the decomposed 5-year yield into expectation component (left panel) and risk premium (right panel) from the functional AFNS model with aggregate life cycle determinant (dashed line) and the AFNS model (dotted line). The results of posterior median are reported for both models. Shaded areas are NBER recessions.

Figure 13. Decomposition of the 5-year yield

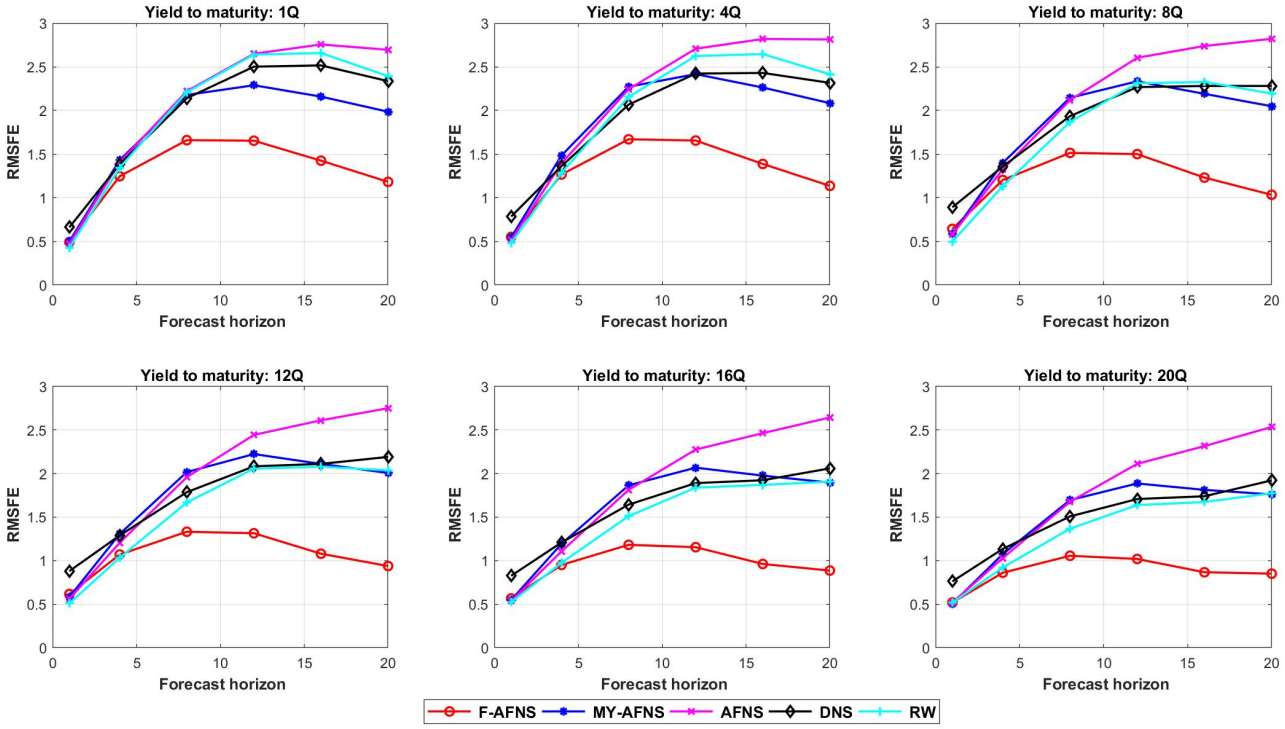

Note: This figure shows out-of-sample forecast comparison on the F-AFNS model with four alternative models of MY-AFNS, AFNS, DNS, and random walk (RW); Each panel shows the 1- to 20-quarter ahead root mean squared forecast errors (RMSFE) for a particular yield to maturity from the five models.

Figure 14. Forecast comparisons based on the RMSFE

Table 1. Parameter estimates based on the MCMC method

Measurement Equations				
Trend				
α_1	α_2	α_3	α_4	α_5
-6.726	**38.134**	-5.402	6.513	**−34.858**
(-32.294, 17.850)	(26.146, 49.491)	(-18.774, 8.521)	(-18.084, 32.103)	(-45.951, -23.144)
Cycle				
	λ	$\mu_l^Q * 10^4$	$\sigma_\epsilon * 4 * 10^4$	
	0.283	**2.998**	**8.276**	
	(0.269, 0.295)	(2.735, 3.326)	(8.013, 8.557)	
State Equations				
Φ	L_{t-1}	S_{t-1}	C_{t-1}	μ
L_t	**0.964**	**0.087**	**−0.053**	0.0002
	(0.925, 1.003)	(0.045, 0.129)	(-0.078, -0.027)	(-0.0000, 0.0004)
S_t	**−0.084**	**0.845**	0.024	**−0.0003**
	(-0.143, -0.025)	(0.783, 0.907)	(-0.014, 0.061)	(-0.0006, -0.0000)
C_t	0.031	**0.423**	**0.591**	**0.0018**
	(-0.105, 0.169)	(0.282, 0.566)	(0.503, 0.677)	(0.0012, 0.0025)
$\Omega * 10^4$	**0.018**			
	(0.015, 0.021)			
	−0.011	**0.041**		
	(-0.015, -0.008)	(0.035, 0.048)		
	-0.007	0.009	**0.211**	
	(-0.015, 0.001)	(-0.001, 0.021)	(0.179, 0.251)	

Note: This table shows the median of the drawn parameters, and the 90% confidence interval in brackets includes the 5% and 95% quantiles of the drawn parameters.

Table 2. Inefficiency factors of parameter posterior draws

Measurement Equations				
Trend				
α_1	α_2	α_3	α_4	α_5
322.492	323.999	322.524	322.476	324.202
Cycle				
	λ	μ_l^Q	σ_ϵ	
	299.639	443.211	1.162	
State Equations				
Φ	L_{t-1}	S_{t-1}	C_{t-1}	μ
L_t	3.159	12.496	9.014	17.074
S_t	1.618	8.998	11.153	9.944
C_t	4.941	2.856	2.943	11.257
Ω	12.902			
	8.702	6.044		
	31.869	19.424	10.113	

Note: The inefficiency factor is defined as in Chib and Ergashev (2009): $1 + 2\sum_{l=1}^{500}(1 - \frac{l}{500})\rho(l)$, where $\rho(l)$ is the sample autocorrelation of lag l for each MCMC sequence.

Table 3. In-sample fit of the F-AFNS model: Residual statistics (bps)

Maturity	Mean	Median	Max	Min	Std	RMSE	MAE
1Q	-0.528	-0.692	20.336	-14.028	3.845	3.874	2.726
4Q	2.117	2.251	42.981	-29.173	9.313	9.533	7.013
8Q	-3.109	-2.809	20.982	-28.902	6.260	6.979	5.256
12Q	0.546	0.026	22.313	-18.720	6.916	6.924	5.374
16Q	2.268	1.847	42.438	-24.265	6.379	6.759	4.688
20Q	-1.299	-1.127	19.070	-31.525	6.938	7.046	5.339
Average	-0.001	-0.084	28.020	-24.435	6.608	6.852	5.066

Note: This table shows the descriptive statistics of the median residuals of the yields.

Table 4. Statistics of the decomposed term structure (%)

	Yields		Trends		Cycles	
Maturity	Mean	Std	Mean	Std	Mean	Std
1Q	4.317	3.090	5.064	2.530	-0.741	1.719
4Q	4.757	3.201	5.011	2.547	-0.275	1.682
8Q	4.957	3.166	4.982	2.570	0.006	1.569
12Q	5.140	3.088	4.955	2.589	0.180	1.488
16Q	5.294	3.030	4.929	2.606	0.342	1.455
20Q	5.404	2.959	4.904	2.619	0.513	1.451
20Q − 1Q	1.087	1.000	-0.161	0.557	1.253	1.239

Note: This table shows the mean and standard deviation of actual yields as well as the median trends and cycles of yields.

Table 5. Correlation between risk premia and real activities

Real activity index	Models	4Q	8Q	12Q	16Q	20Q
IP growth	F-AFNS	0.009	-0.057	**−0.106**	**−0.136**	**−0.152**
		(-0.040,0.059)	(-0.108,0.003)	(-0.148,-0.049)	(-0.170,-0.088)	(-0.182,-0.113)
	AFNS	**0.051**	0.012	-0.017	-0.034	-0.042
		(0.011,0.093)	(-0.034,0.060)	(-0.063,0.033)	(-0.079,0.014)	(-0.088,0.001)
Real consumption growth	F-AFNS	**0.078**	-0.019	**−0.096**	**−0.146**	**−0.176**
		(0.013,0.143)	(-0.088,0.069)	(-0.155,-0.006)	(-0.192,-0.066)	(-0.215,-0.109)
	AFNS	**0.159**	**0.124**	**0.093**	**0.072**	**0.059**
		(0.124,0.194)	(0.080,0.168)	(0.047,0.143)	(0.027,0.122)	(0.015,0.106)
Real GDP growth	F-AFNS	**0.084**	0.001	-0.065	**−0.107**	**−0.133**
		(0.026,0.141)	(-0.065,0.076)	(-0.123,0.011)	(-0.156,-0.041)	(-0.175,-0.077)
	AFNS	**0.139**	**0.093**	0.058	0.037	0.026
		(0.093,0.182)	(0.033,0.149)	(-0.010,0.119)	(-0.034,0.097)	(-0.049,0.083)

Note: This table shows the median of the correlations between risk premia and real activity indices, and the 95% confidence interval in brackets include the 2.5% and 97.5% quantile of correlation.